

---

# A WELL-BALANCED SECOND-ORDER FINITE VOLUME APPROXIMATION FOR A COUPLED SYSTEM OF GRANULAR FLOW

---

A PREPRINT

**Aekta Aggarwal**

Operations Management and Quantitative Techniques  
Indian Institute of Management Indore  
Indore-453556  
aektaaggarwal@iimidr.ac.in

**Veerappa Gowda G. D.**

Centre for Applicable Mathematics  
Tata Institute of Fundamental Research  
Bangalore – 560065  
gowda@tifrbng.res.in

**Sudarshan Kumar K.\***

School of Mathematics  
Indian Institute of Science Education and Research  
Trivandrum –695551  
sudarshan@iisertvm.ac.in

January 4, 2024

This paper is dedicated to Prof. Adimurthi on the occasion of his 70th birthday

## ABSTRACT

A well-balanced second-order finite volume scheme is proposed and analyzed for a  $2 \times 2$  system of non-linear partial differential equations which describes the dynamics of growing sandpiles created by a vertical source on a flat, bounded rectangular table in multiple dimensions. To derive a second-order scheme, we combine a MUSCL type spatial reconstruction with strong stability preserving Runge-Kutta time stepping method. The resulting scheme is ensured to be well-balanced through a modified limiting approach that allows the scheme to reduce to well-balanced first-order scheme near the steady state while maintaining the second-order accuracy away from it. The well-balanced property of the scheme is proven analytically in one dimension and demonstrated numerically in two dimensions. Additionally, numerical experiments reveal that the second-order scheme reduces finite time oscillations, takes fewer time iterations for achieving the steady state and gives sharper resolutions of the physical structure of the sandpile, as compared to the existing first-order schemes of the literature.

**Keywords** Hamilton Jacobi equations · Well-Balanced schemes · Discontinuous Flux · Sandpile · Balance Laws

## 1 Introduction

The study of granular matter dynamics has been gaining interest among applied mathematicians in the last few years. A wide array of models can be found in the literature, ranging from kinetic models to hyperbolic differential equations. For detailed discussion of these models, refer to [22] and the references therein. This area of research has seen numerous endeavors focusing on the theoretical aspects of differential equations, as evidenced by works such as [12–14, 16, 18, 29, 32]. Additionally, considerable efforts have been devoted to the numerical approximation of these proposed models, as seen in [1, 3, 20, 21].

In this work, our focus is on the model equations introduced in [29], commonly referred to as the Hadler and Kuttler (**HK**) model. This model comprises of a coupled system of non-linear partial differential equations and is widely

---

\*Corresponding author

recognized for describing the evolution of a sandpile formed by pouring dry sand grains onto a flat and bounded table surface denoted as  $\Omega$ . The evolution of sandpile is governed by these equations under the influence of a time-independent non-negative vertical source represented by  $f \in L^1(\Omega)$ . It is assumed that all sand grains are uniform in size, thus disregarding phenomena like segregation or pattern formation. Additionally, external factors such as wind or stress fields within the bulk of the medium are not taken into account. The **(HK)** model reads as:

$$u_t = (1 - |\nabla u|)v, \quad \text{in } \Omega \times (0, T] \quad (1)$$

$$v_t - \nabla \cdot (v \nabla u) = -(1 - |\nabla u|)v + f, \quad \text{in } \Omega \times (0, T] \quad (2)$$

$$u(\mathbf{x}, 0) = u_0(\mathbf{x}), \quad v(\mathbf{x}, 0) = v_0(\mathbf{x}), \quad \text{in } \Omega \quad (3)$$

where at any point  $(\mathbf{x}, t) \in \Omega \times [0, T]$ ,  $u(\mathbf{x}, t)$  denotes the local height of the pile containing the grains at rest and is called the *standing* layer, and  $v(\mathbf{x}, t)$  denotes the *rolling* layer, formed by the grains that roll on the surface of the pile until they are captured by the standing layer. Further, the boundary  $\partial\Omega$  can be split into two parts:  $\Gamma_o$ , an open non-empty subset of  $\partial\Omega$  where the sand can fall down from the table and  $\Gamma_w = \partial\Omega \setminus \Gamma_o$  where the sand is blocked by a wall. From modelling point of view, a wall of arbitrary height can be imagined on  $\Gamma_w$  so that no sand can trespass this wall, while on  $\Gamma_o$ , the table is “open”. If  $\Gamma_o = \partial\Omega$ , then the problem is called as *open table problem*, otherwise it is called *partially open table problem*. The system (1)-(2) is supplemented with the following boundary conditions:

$$u = 0 \quad \text{in } \Gamma_o, \quad v \frac{\partial u}{\partial \nu} = 0 \quad \text{in } \Gamma_w \quad (4)$$

a detailed discussion can be found in [1, 3, 20, 29]. For stability reasons,  $|\nabla u|$  cannot exceed 1. Moreover, at any equilibrium, the profile of  $|\nabla u|$  must be maximal where transport occurs (that is, where  $v > 0$ ). The exchange of the grains between the two layers occurs through an exchange term  $(|\nabla u| - 1)v$  which is independent of the slope orientation and can be characterized as erosion/deposition. The equilibrium of the system (1)-(4) is given by:

$$\begin{aligned} -\nabla \cdot (v \nabla u) &= f, \quad \text{in } \Omega, \\ |\nabla u| &= 1, \quad \text{on } \{v > 0\} \\ |\nabla u| &\leq 1, \quad u, v \geq 0, \quad \text{in } \Omega \\ u &= 0 \quad \text{in } \Gamma_o, \quad v \frac{\partial u}{\partial \nu} = 0 \quad \text{in } \Gamma_w \end{aligned} \quad (5)$$

A complete mathematical theory for the existence of solutions of **(HK)** model at finite time and at equilibrium is still not completely settled and is not covered by standard existence and uniqueness results available for hyperbolic balance laws, see [4, 5, 12–14, 29, 33] for some limited results. Recent attention has also been devoted to exploring the slow erosion limit of the model in one dimension, as evident in [6, 9, 15, 17, 28] and references therein. In the past decade, numerous studies have aimed to develop robust numerical schemes approximating **(HK)** model, with the ability to preserve the discrete steady states and the physical properties of the model efficiently, see [1, 3, 20, 22]. In this context, finite difference schemes capturing the discrete steady states were proposed and analyzed in [20, 22] and well-balanced finite volume schemes were developed in [1, 3] using the basic principle of conservation laws with discontinuous flux. The class of finite volume schemes based on conservation laws with discontinuous flux have been used in the last decade for various real life applications, see [2, 10, 11, 34]. The schemes proposed in [1, 3] were shown to be well-balanced and capable of capturing the sharp crests at the equilibrium state more efficiently than existing methods. However, these schemes exhibited oscillations near the initial condition, persisting for a significant duration, leading to a delay in reaching the steady state. This issues give rise to an important question: is it possible to control these oscillations and reduce the time taken to reach the steady state by moving to a high-order scheme? Simultaneously, it also put forth the question of whether these high-order scheme could result in a sharper resolution of the discrete steady state.

In various scenarios, the well-balanced schemes for hyperbolic systems have been of keen interest over the past few decades, see [7, 8, 19, 23, 24, 27, 30, 31] and the references therein. It has been observed that capturing moving steady states or those with complex structures, like that of (5), can be a challenging task in general. To the best of our knowledge, there have been no studies on second-order schemes for (5) in the existing literature. However, in the case of shallow water equations, second-order schemes were proposed and analyzed in [19, 31]. It has been noted in these studies that the second-order extensions may not inherently possess the well-balanced characteristics, and an adaptation algorithm is required to ensure this property. In this work to derive a second-order scheme we employ a MUSCL-type spatial reconstruction [35] along with a strong stability preserving Runge-Kutta time stepping method [25, 26], which is basically an extension of the first-order scheme of [1, 3]. In Section 4, we illustrate that this second-order scheme is not well-balanced for the state variable  $v$ . To overcome this difficulty, we modify the proposed second-order scheme with an adaptation procedure similar to that of [19], to develop a well-balanced second-order scheme. The procedure involves a modified limitation strategy in the linear reconstruction of the approximate solution at each time step. We establish that the resulting scheme is well-balanced and is able to accurately capture the discrete steady state.

The rest of this paper is organized as follows. In Section 2, we focus on deriving the second-order numerical scheme and provide a concise overview of the first-order numerical scheme proposed in [1, 3]. The stability analysis for the second-order scheme is presented in Section 3. A discussion about the well-balance property of the second-order scheme is outlined in Section 4. In Section 5, we elucidate the second-order adaptive scheme and analytically establish its well-balance property. Section 6 deals with the extension of the first-order scheme from one dimension to two dimensions, along with the adaptation procedure in the two-dimensional context. In Section 7, we provide numerical examples in both one and two dimensions to showcase the performance of the proposed second-order adaptive scheme in comparison to the non-adaptive second-order scheme and the first-order schemes of [1, 3]. We finally draw our conclusion in Section 8.

## 2 Numerical schemes in one-dimension

We now present the numerical algorithm approximating (1)-(2) in one dimension. First, we briefly review the first-order finite volume schemes of [1, 3] and then present the second-order scheme. Let  $\Omega := (0, 1)$ . As in [1], we rewrite (1)-(3) as follows:

$$u_t + F_1(\alpha, v) = 0, \quad \text{in } \Omega \times (0, T] \quad (6)$$

$$v_t + F_2(\alpha, v, B)_x - F_1(\alpha, v) = 0, \quad \text{in } \Omega \times (0, T] \quad (7)$$

$$u(x, 0) = v(x, 0) = 0, \quad \text{in } \Omega$$

where  $\alpha = u_x$ ,  $B(x) = \int_0^x f(\xi)d\xi$ ,  $F_1(\alpha, v) = (|\alpha| - 1)v$ , and  $F_2(\alpha, v, B) = -\alpha v - B(x)$ . For  $\Delta x, \Delta t > 0$ , we define  $\lambda := \Delta t/\Delta x$  and consider equidistant spatial grid points  $x_{i+\frac{1}{2}} := i\Delta x$ , for non-negative integers  $i \in \mathcal{M} := \{0, 1, \dots, M\}$  and temporal grid points  $t^n := n\Delta t$  for non-negative integer  $n \in \mathcal{N}_T := \{0, 1, \dots, N_T\}$ , such that  $x_{\frac{1}{2}} = 0$ ,  $x_{M+\frac{1}{2}} = 1$  and  $T = t^{N_T}$ . Let  $x_i = \frac{1}{2}(x_{i+\frac{1}{2}} + x_{i-\frac{1}{2}})$  for  $i \in \{1, \dots, M\}$ . We also denote the cell  $C_i^n := C_i \times C^n$ , where  $C_i := [x_{i-\frac{1}{2}}, x_{i+\frac{1}{2}})$  and  $C^n := [t^n, t^{n+1})$ . Let  $u_{i+\frac{1}{2}}^n$  be an approximation of the solution  $u$  calculated at grid points  $x_{i+\frac{1}{2}}$  at time  $t^n$ . For each  $(i, n) \in \mathcal{M} \times \mathcal{N}_T$ , define

$$\alpha_i^n := \frac{u_{i+\frac{1}{2}}^n - u_{i-\frac{1}{2}}^n}{\Delta x} \quad \text{and} \quad v_i^n := \frac{1}{\Delta x} \int_{C_i} v(x, t^n) dx$$

as the approximation for  $\alpha, v$  in the cell  $C_i^n$ . Also, following [3] we use the notation  $D_f := \overline{\{x : f(x) \neq 0\}}$ .

### 2.1 First-order scheme

The first-order finite volume scheme for the system (1)-(2), formulated in [1, 3] is given by

$$\begin{aligned} u_{i+\frac{1}{2}}^{n+1} &= u_{i+\frac{1}{2}}^n - \Delta t G_{i+\frac{1}{2}}^n, \quad (i, n) \in (\mathcal{M} \setminus \{M, 0\}) \times \mathcal{N}_T \\ v_i^{n+1} &= v_i^n - \lambda(H_{i+\frac{1}{2}}^n - H_{i-\frac{1}{2}}^n) + \Delta t S_i^n, \quad (i, n) \in (\mathcal{M} \setminus \{0\}) \times \mathcal{N}_T \end{aligned} \quad (8)$$

Here, the terms  $G_{i+\frac{1}{2}}^n$  and  $H_{i+\frac{1}{2}}^n$  are the numerical fluxes associated with the fluxes  $F_1$  and  $F_2$ , respectively at  $(x_{i+\frac{1}{2}}, t^n)$  and are given by:

$$G_{i+\frac{1}{2}}^n = G(\alpha_i^n, v_i^n, \alpha_{i+1}^n, v_{i+1}^n), \quad H_{i+\frac{1}{2}}^n = H(\alpha_i^n, v_i^n, \alpha_{i+1}^n, v_{i+1}^n, B_i, B_{i+1})$$

with

$$G(a, b, c, d) = \max\{(|\max\{a, 0\}| - 1)b, (|\min\{c, 0\}| - 1)d\} \quad (9)$$

$$H(a, b, c, d, e_1, e_2) = \begin{cases} (-ab - e_1), & -a \geq 0, -c \geq 0 \\ (-cd - e_2), & -a < 0, -c \leq 0 \\ \frac{-ce_1 + ae_2}{(c-a)}, & -a < 0, -c > 0 \\ (-ab - e_1), & b > d \text{ and } -a \geq 0, -c \leq 0 \\ (-cd - e_2), & b < d, \text{ and } -a \geq 0, -c \leq 0 \\ -\frac{1}{2}(ab + cd + e_1 + e_2), & b = d \text{ and } -a \geq 0, -c \leq 0 \end{cases} \quad (10)$$

The term  $S_i^n$  is given as

$$S_i^n = v_i^n (|\alpha_i^n| - 1)$$

The scheme (8) is implemented with initial conditions given by  $u_{i+\frac{1}{2}}^0 = 0$ , for all  $i \in \mathcal{M}$  and  $v_i^0 = 0$ , for all  $i \in \mathcal{M} \setminus \{0\}$ . Regarding the boundary conditions, we mainly consider two types: open table ( $\Gamma_o = \{0, 1\}$ ) and partially open table ( $\Gamma_o = \{0\}$ ). In each case, the boundary conditions are specified as follows:

Boundary condition for  $u$  :

- $\Gamma_o = \{0, 1\}$  :

$$u_{\frac{1}{2}}^n = u_{M+\frac{1}{2}}^n = 0$$

- $\Gamma_o = \{0\}$  :

$$u_{\frac{1}{2}}^n = 0, \quad u_{M+\frac{1}{2}}^{n+1} = \begin{cases} u_{M-\frac{1}{2}}^n & \text{if } D_f = [X_1, X_2], X_2 < 1 \\ u_{M-\frac{1}{2}}^n + \Delta x \max(\alpha_{M-1}^n, 0) & \text{if } D_f = [X_1, X_2], X_2 = 1 \end{cases}$$

Boundary conditions for  $v$  : The boundary condition for  $v$  are set through the fluxes as done in [1, 3].

- $\Gamma_o = \{0, 1\}$  :

$$H_{\frac{1}{2}}^n = -\alpha_1^n v_1^n - B_1, \quad H_{M+\frac{1}{2}}^n = -\alpha_M^n v_M^n - B_M$$

- $\Gamma_o = \{0\}$  :

$$H_{\frac{1}{2}}^n = -\alpha_1^n v_1^n - B_1, \quad H_{M+\frac{1}{2}}^n = \begin{cases} -\alpha_M^n v_M^n - B_M & \text{if } \alpha_M^n \leq 0 \\ -B_{M+1} & \text{if } \alpha_M^n > 0 \end{cases} \quad (11)$$

## 2.2 Second-order scheme

We now describe the second-order extension of the first-order scheme described in the previous section. To construct a second-order scheme, we employ a MUSCL type spatial reconstruction and a two stage strong stability preserving Runge-Kutta method in time. To begin with, in each cell  $C_i$ , we construct a piecewise linear function  $z_{\Delta x}$  which is defined by

$$z_{\Delta x}(x, t) := z_i^n + \frac{(x - x_i)}{\Delta x} (z_{i+\frac{1}{2},L}^n - z_{i-\frac{1}{2},R}^n), \quad z = \alpha, v \text{ and } B$$

where

$$z_{i+\frac{1}{2},L}^n = z_i^n + \frac{1}{2} D z_i^n, \quad z_{i-\frac{1}{2},R}^n = z_i^n - \frac{1}{2} D z_i^n \quad (12)$$

and

$$D z_i^n = 2\theta \min\text{mod} \left( z_i^n - z_{i-1}^n, \frac{1}{2} (z_{i+1}^n - z_{i-1}^n), z_{i+1}^n - z_i^n \right), \quad \theta \in [0, 1] \quad (13)$$

represent the slopes obtained using the minmod limiter, where the minmod function is defined as

$$\min\text{mod}(a_1, \dots, a_m) := \begin{cases} \text{sgn}(a_1) \min_{1 \leq k \leq m} \{|a_k|\}, & \text{if } \text{sgn}(a_1) = \dots = \text{sgn}(a_m) \\ 0, & \text{otherwise} \end{cases} \quad (14)$$

Note that  $\theta = 0$  in (11) gives the first-order scheme, while  $\theta = 0.5$  gives the usual minmod limiter. For each  $i$ , we can find  $\sigma_i^L$  and  $\sigma_i^R$  with  $0 \leq \sigma_i^L, \sigma_i^R \leq 1$  such that

$$z_{i+\frac{1}{2},L}^n = z_i^n + \theta \sigma_i^R (z_{i+1}^n - z_i^n), \quad z_{i+\frac{1}{2},R}^n = z_{i+1}^n - \theta \sigma_{i+1}^L (z_{i+1}^n - z_i^n) \quad (15)$$

This ensures that for all  $0 \leq \theta \leq 1$ ,

$$\min\{z_i^n, z_{i+1}^n\} \leq z_{i+\frac{1}{2},L}^n, z_{i+\frac{1}{2},R}^n \leq \max\{z_i^n, z_{i+1}^n\}$$

The time steps of the second-order scheme using the Runge-Kutta method are defined as follows:

**RK step-1:** Define

$$\begin{aligned} u_{i+\frac{1}{2}}^{n,*} &:= u_{i+\frac{1}{2}}^n - \Delta t G_{i+\frac{1}{2}}^n \\ v_i^{n,*} &:= v_i^n - \lambda (H_{i+\frac{1}{2}}^n - H_{i-\frac{1}{2}}^n) + \Delta t S_{i+\frac{1}{2},L}^n \end{aligned} \quad (16)$$

where

$$\begin{aligned} G_{i+\frac{1}{2}}^n &= G(\alpha_{i+\frac{1}{2},L}^n, v_{i+\frac{1}{2},L}^n, \alpha_{i+\frac{1}{2},R}^n, v_{i+\frac{1}{2},R}^n) \\ H_{i+\frac{1}{2}}^n &= H(\alpha_{i+\frac{1}{2},L}^n, v_{i+\frac{1}{2},L}^n, \alpha_{i+\frac{1}{2},R}^n, v_{i+\frac{1}{2},R}^n, B_{i+\frac{1}{2},L}, B_{i+\frac{1}{2},R}) \\ S_{i+\frac{1}{2},L}^n &= -g(\alpha_{i+\frac{1}{2},L}^n, v_{i+\frac{1}{2},L}^n) \end{aligned}$$

and  $g(a, b) = (|a| - 1)b$ . Also, we have

$$\alpha_i^{n,*} = \frac{u_{i+\frac{1}{2}}^{n,*} - u_{i-\frac{1}{2}}^{n,*}}{\Delta x} \quad (17)$$

**RK step-2:** Given the values  $\alpha_i^{n,*}$  and  $v_i^{n,*}$  from RK step-1, we proceed to construct corresponding  $\alpha_{i+\frac{1}{2},L}^{n,*}$ ,  $\alpha_{i+\frac{1}{2},R}^{n,*}$ ,  $v_{i+\frac{1}{2},L}^{n,*}$  and  $v_{i+\frac{1}{2},R}^{n,*}$  by using (12)-(13) for  $z = \alpha^*$ ,  $v^*$  and  $B^*$ . Here, we define

$$\begin{aligned} u_{i+\frac{1}{2}}^{n,**} &:= u_{i+\frac{1}{2}}^{n,*} - \lambda(G_{i+\frac{1}{2}}^{n,*} - G_{i-\frac{1}{2}}^{n,*}) \\ v_i^{n,**} &:= v_i^{n,*} - \lambda(H_{i+\frac{1}{2}}^{n,*} - H_{i-\frac{1}{2}}^{n,*}) + \Delta t S_{i+\frac{1}{2},L}^{n,*} \end{aligned}$$

where

$$\begin{aligned} G_{i+\frac{1}{2}}^{n,*} &= G(\alpha_{i+\frac{1}{2},L}^{n,*}, v_{i+\frac{1}{2},L}^{n,*}, \alpha_{i+\frac{1}{2},R}^{n,*}, v_{i+\frac{1}{2},R}^{n,*}) \\ H_{i+\frac{1}{2}}^{n,*} &= H(\alpha_{i+\frac{1}{2},L}^{n,*}, v_{i+\frac{1}{2},L}^{n,*}, \alpha_{i+\frac{1}{2},R}^{n,*}, v_{i+\frac{1}{2},R}^{n,*}, B_{i+\frac{1}{2},L}, B_{i+\frac{1}{2},R}) \\ S_{i+\frac{1}{2},L}^{n,*} &= -g(\alpha_{i+\frac{1}{2},L}^{n,*}, v_{i+\frac{1}{2},L}^{n,*}) \end{aligned}$$

Finally, the second-order scheme is written as

$$\begin{aligned} u_{i+\frac{1}{2}}^{n+1} &= \frac{1}{2}(u_{i+\frac{1}{2}}^n + u_{i+\frac{1}{2}}^{n,**}) \\ v_i^{n+1} &= \frac{1}{2}(v_i^n + v_i^{n,**}) \end{aligned} \quad (18)$$

### 2.3 Boundary conditions for the second-order scheme

Case 1: (open table problem,  $\Gamma_0 = \{0, 1\}$ ) in the second-order case, the computation of fluxes for  $i = \frac{3}{2}$  and  $i = M - \frac{1}{2}$  requires the ghost cell values for the linear reconstruction. To simplify this, we set the slopes  $Dz_i^n$  in the first and last cells to zero. Further, the boundary condition for  $u$  is implemented in the same way as in the first-order scheme given in Section 2.1, specifically for grids corresponding to  $i = \frac{1}{2}$  and  $M + \frac{1}{2}$ . Similarly for the case of  $v$ .

Case 2: (partially open table problem with  $\Gamma_0 = \{0\}$ ) in this case as well, we set the slopes  $Dz_i^n$  in the first and last cells to zero, and the boundary conditions for  $u$  and  $v$  at the left boundary, where  $x = 0$  are same as the first-order case in Section 2.1. At the right boundary, where  $x = 1$ , the boundary condition for  $v$  remains the same as in Section 2.1. However, the approximation for  $u$  at this boundary is evolved as

$$u_{M+\frac{1}{2}}^{n+1} = \begin{cases} u_{M-\frac{1}{2}}^n, & \text{if } D_f = [X_1, X_2], X_2 < 1 \\ u_{M-\frac{1}{2}}^n + \Delta x \max(\alpha_{M-\frac{1}{2},L}^n, 0), & \text{if } D_f = [X_1, X_2], X_2 = 1 \end{cases}$$

## 3 Stability results in one-dimension

In this section, we show that the numerical solutions obtained using the second-order scheme (18) satisfy the physical properties in the case of open table problem. Similarly, one can derive the results for the partially open table problem.

**Theorem 1** *Let  $f \geq 0$  in  $\Omega$ . Assume that  $\sup_{i \in \mathbb{Z}} |\alpha_i^0| \leq 1$ ,  $u_{i+\frac{1}{2}}^0 \geq 0$  and  $v_i^0 \geq 0$ , for all  $i \in \mathbb{Z}$ , then the numerical scheme (18) under the CFL conditions:*

$$\lambda \max_i v_i^n \leq \frac{1}{2}, \quad (19)$$

$$\lambda \leq \frac{1}{2} - \Delta t \quad (20)$$

*satisfies the following properties for all  $i \in \mathbb{Z}$ :*

$$(i) \sup_{i \in \mathbb{Z}} |\alpha_i^{n+1}| \leq 1, u_{i+\frac{1}{2}}^{n+1} \geq u_{i+\frac{1}{2}}^n \geq 0$$

$$(ii) v_i^{n+1} \geq 0$$

**Proof** From (17) we can write

$$\begin{aligned} \alpha_i^{n,*} &= \frac{1}{2}(\alpha_{i+\frac{1}{2},L}^n + \alpha_{i-\frac{1}{2},R}^n) - \lambda(G_{i+1/2}^n - G_{i-1/2}^n) \\ &= K_1(\alpha_{i-\frac{1}{2},L}^n, \alpha_{i-\frac{1}{2},R}^n, \alpha_{i+\frac{1}{2},L}^n, \alpha_{i+\frac{1}{2},R}^n, v_{i-\frac{1}{2},L}^n, v_{i-\frac{1}{2},R}^n, v_{i+\frac{1}{2},L}^n, v_{i+\frac{1}{2},R}^n) \end{aligned}$$

Now, we aim to show that  $K_1$  is non-decreasing in  $\alpha_{i\pm\frac{1}{2},L}^n$  and  $\alpha_{i\pm\frac{1}{2},R}^n$  under the CFL conditions (19). For each  $i$ , we have

$$\begin{aligned} \frac{\partial G_{i+\frac{1}{2}}^n}{\partial \alpha_{i-\frac{1}{2},L}^n} &= 0 \\ \frac{\partial G_{i+\frac{1}{2}}^n}{\partial \alpha_{i+\frac{1}{2},L}^n} &= \begin{cases} v_{i+\frac{1}{2},L}^n & \text{if } G_{i+\frac{1}{2}}^n = (|\max(\alpha_{i+\frac{1}{2},L}^n, 0)| - 1)v_{i+\frac{1}{2},L}^n \text{ and } \alpha_{i+\frac{1}{2},L}^n > 0 \\ 0 & \text{otherwise} \end{cases} \end{aligned}$$

and

$$\frac{\partial G_{i+\frac{1}{2}}^n}{\partial \alpha_{i+\frac{1}{2},R}^n} = \begin{cases} -v_{i+\frac{1}{2},R}^n & \text{if } G_{i+\frac{1}{2}}^n = (|\min(\alpha_{i+\frac{1}{2},R}^n, 0)| - 1)v_{i+\frac{1}{2},R}^n \text{ and } \alpha_{i+\frac{1}{2},R}^n < 0 \\ 0 & \text{otherwise} \end{cases}$$

This shows that  $G_{i+\frac{1}{2}}^n$  is non-decreasing in  $\alpha_{i+\frac{1}{2},L}^n$  and non-increasing in  $\alpha_{i+\frac{1}{2},R}^n$ . Hence, we have

$$\frac{\partial K_1}{\partial \alpha_{i-\frac{1}{2},L}^n} = \lambda \frac{\partial G_{i-\frac{1}{2}}^n}{\partial \alpha_{i-\frac{1}{2},L}^n} \geq 0 \text{ and } \frac{\partial K_1}{\partial \alpha_{i+\frac{1}{2},R}^n} = -\lambda \frac{\partial G_{i+\frac{1}{2}}^n}{\partial \alpha_{i+\frac{1}{2},R}^n} \geq 0$$

Further, using the CFL condition (19), it yields

$$\frac{\partial K_1}{\partial \alpha_{i+\frac{1}{2},L}^n} = \frac{1}{2} - \lambda \frac{\partial G_{i+\frac{1}{2}}^n}{\partial \alpha_{i+\frac{1}{2},L}^n} = \frac{1}{2} - \lambda v_{i+\frac{1}{2},L}^n \geq 0 \text{ and } \frac{\partial K_1}{\partial \alpha_{i-\frac{1}{2},R}^n} = \frac{1}{2} + \lambda \frac{\partial G_{i-1/2}^n}{\partial \alpha_{i-\frac{1}{2},R}^n} = \frac{1}{2} - \lambda v_{i-\frac{1}{2},R}^n \geq 0$$

This proves that  $K_1$  is increasing in each of its variables  $\alpha_{i\pm\frac{1}{2},L}^n$  and  $\alpha_{i\pm\frac{1}{2},R}^n$  under the CFL condition (19). Thus we can write

$$\begin{aligned} -1 &= K_1(-1, -1, -1, -1, v_{i-\frac{1}{2},L}^n, v_{i-\frac{1}{2},R}^n, v_{i+\frac{1}{2},L}^n, v_{i+\frac{1}{2},R}^n) \\ &\leq K_1(\alpha_{i-\frac{1}{2},L}^n, \alpha_{i-\frac{1}{2},R}^n, \alpha_{i+\frac{1}{2},L}^n, \alpha_{i+\frac{1}{2},R}^n, v_{i-\frac{1}{2},L}^n, v_{i-\frac{1}{2},R}^n, v_{i+\frac{1}{2},L}^n, v_{i+\frac{1}{2},R}^n) \\ &= \alpha_i^{n,*} \leq K_1(1, 1, 1, 1, v_{i-\frac{1}{2},L}^n, v_{i-\frac{1}{2},R}^n, v_{i+\frac{1}{2},L}^n, v_{i+\frac{1}{2},R}^n) = 1 \end{aligned}$$

i.e.,

$$-1 \leq \alpha_i^{n,*} \leq 1$$

By setting

$$\alpha_i^{n,**} = K_1(\alpha_{i-1/2L}^{n,*}, \alpha_{i-1/2R}^{n,*}, \alpha_{i+\frac{1}{2},L}^{n,*}, \alpha_{i+\frac{1}{2},R}^{n,*}, v_{i-\frac{1}{2},L}^{n,*}, v_{i-\frac{1}{2},R}^{n,*}, v_{i+\frac{1}{2},L}^{n,*}, v_{i+\frac{1}{2},R}^{n,*})$$

under the CFL condition (19), it can be similarly shown that

$$-1 \leq \alpha_i^{n,**} \leq 1$$

Since

$$\alpha_i^{n+1} = \frac{1}{2}(\alpha_i^n + \alpha_i^{n,**})$$

it follows that

$$-1 \leq \alpha_i^{n+1} \leq 1$$

under the CFL condition (19). Note that  $G_{i+\frac{1}{2}}^n \leq 0$  as we have  $-1 \leq \alpha_{i\pm\frac{1}{2},L}^n, \alpha_{i\pm\frac{1}{2},R}^n \leq 1$ . Consequently, from the expression

$$u_{i+\frac{1}{2}}^{n,*} = u_{i+\frac{1}{2}}^n - \Delta t G_{i+\frac{1}{2}}^n$$

it gives that  $u_{i+\frac{1}{2}}^{n,*} \geq u_{i+\frac{1}{2}}^n$ . In the similar way, given that  $-1 \leq \alpha_{i\pm\frac{1}{2},L}^{n,*}, \alpha_{i\pm\frac{1}{2},R}^{n,*} \leq 1$ , we can see that  $u_{i+\frac{1}{2}}^{n,**} \geq u_{i+\frac{1}{2}}^{n,*} \geq u_{i+\frac{1}{2}}^n$ . Further,

$$u_{i+\frac{1}{2}}^{n+1} = \frac{1}{2}(u_{i+\frac{1}{2}}^n + u_{i+\frac{1}{2}}^{n,**}) \geq u_{i+\frac{1}{2}}^n$$

This proves (i).

Now, let us consider the equation

$$v_i^{n,*} = v_i^n - \lambda(H_{i+\frac{1}{2}}^n - H_{i-\frac{1}{2}}^n) + \Delta t v_{i+\frac{1}{2},L}^n (|\alpha_{i+\frac{1}{2},L}^n| - 1)$$

and denote

$$v_i^{n,*} = K_2(\alpha_{i-\frac{1}{2},L}^n, \alpha_{i-\frac{1}{2},R}^n, \alpha_{i+\frac{1}{2},L}^n, \alpha_{i+\frac{1}{2},R}^n, v_{i-\frac{1}{2},L}^n, v_{i-\frac{1}{2},R}^n, v_{i+\frac{1}{2},L}^n, v_{i+\frac{1}{2},R}^n)$$

To prove that  $K_2$  is non-decreasing in each variables  $v_{i\pm\frac{1}{2},L}^n$  and  $v_{i\pm\frac{1}{2},R}^n$ , we consider the following two cases and other cases follow in a similar manner.

**Case 1:**  $-\alpha_{i\pm\frac{1}{2},L}^n \geq 0, -\alpha_{i\pm\frac{1}{2},R}^n \geq 0$ . With these condition, the numerical fluxes now read as

$$H_{i\pm\frac{1}{2}}^n = -\alpha_{i\pm\frac{1}{2},L}^n v_{i\pm\frac{1}{2},L}^n - B_{i\pm\frac{1}{2},L}$$

and we have

$$\begin{aligned} K_2 &= \frac{1}{2}(v_{i+\frac{1}{2},L}^n + v_{i-\frac{1}{2},R}^n) - \lambda(-\alpha_{i+\frac{1}{2},L}^n v_{i+\frac{1}{2},L}^n - B_{i+\frac{1}{2},L}) \\ &\quad + \lambda(-\alpha_{i-\frac{1}{2},L}^n v_{i-\frac{1}{2},L}^n - B_{i-\frac{1}{2},L}) + \Delta t v_{i+\frac{1}{2},L}^n (|\alpha_{i+\frac{1}{2},L}^n| - 1) \end{aligned}$$

Upon differentiation, we find:

$$\begin{aligned} \frac{\partial K_2}{\partial v_{i-\frac{1}{2},L}^n} &= \frac{\partial H_{i-\frac{1}{2}}^n}{\partial v_{i-\frac{1}{2},L}^n} = -\lambda \alpha_{i-\frac{1}{2},L}^n \geq 0 \\ \frac{\partial K_2}{\partial v_{i+\frac{1}{2},R}^n} &= 0, \quad \frac{\partial K_2}{\partial v_{i-\frac{1}{2},R}^n} = \frac{1}{2} \\ \frac{\partial K_2}{\partial v_{i+\frac{1}{2},L}^n} &= \frac{1}{2} - \lambda(-\alpha_{i+\frac{1}{2},K_2}^n) + \Delta t (|\alpha_{i+\frac{1}{2},L}^n| - 1) \\ &= \frac{1}{2} - \lambda |\alpha_{i+\frac{1}{2},L}^n| + \Delta t (|\alpha_{i+\frac{1}{2},L}^n| - 1) \end{aligned}$$

Further, together with the CFL condition (20) and the assumption  $|\alpha_{i+\frac{1}{2},L}^n| \leq 1$ , it is easy to see that

$$|\alpha_{i+\frac{1}{2},L}^n| \lambda \leq \frac{1}{2} + \Delta t (|\alpha_{i+\frac{1}{2},L}^n| - 1)$$

This inequality leads to  $\frac{\partial K_2}{\partial v_{i+\frac{1}{2},L}^n} \geq 0$  in the above expressions. Therefore, it can be concluded that under the CFL

condition (20)  $K_2$  is non-decreasing in each of its variables  $v_{i\pm\frac{1}{2},L}^n$  and  $v_{i\pm\frac{1}{2},R}^n$ .

**Case 2:**  $-\alpha_{i-\frac{1}{2},L}^n \geq 0, -\alpha_{i+\frac{1}{2},L}^n \leq 0, -\alpha_{i\pm\frac{1}{2},R}^n \leq 0$ . We prove for the case  $-\alpha_{i-\frac{1}{2},R}^n < 0$  and  $v_{i-\frac{1}{2},R}^n = v_{i-\frac{1}{2},L}^n$ , and other cases can be proved similarly. The numerical fluxes are given by

$$\begin{aligned} H_{i+\frac{1}{2}}^n &= -\alpha_{i+\frac{1}{2},R}^n v_{i+\frac{1}{2},R}^n - B_{i+\frac{1}{2},R} \\ H_{i-\frac{1}{2}}^n &= \frac{1}{2}(-\alpha_{i-\frac{1}{2},L}^n v_{i-\frac{1}{2},L}^n - B_{i-\frac{1}{2},L} - \alpha_{i-\frac{1}{2},R}^n v_{i-\frac{1}{2},R}^n - B_{i-\frac{1}{2},R}) \end{aligned}$$

and

$$\begin{aligned} K_2 &= \frac{1}{2}(v_{i+\frac{1}{2},L}^n + v_{i-\frac{1}{2},R}^n) + \frac{\lambda}{2}(-\alpha_{i-\frac{1}{2},L}^n v_{i-\frac{1}{2},L}^n - B_{i-\frac{1}{2},L} - \alpha_{i-\frac{1}{2},R}^n v_{i-\frac{1}{2},R}^n - B_{i-\frac{1}{2},R}) \\ &\quad - \lambda(-\alpha_{i+\frac{1}{2},R}^n v_{i+\frac{1}{2},R}^n - B_{i+\frac{1}{2},R}) + \Delta t v_{i+\frac{1}{2},L}^n (\alpha_{i+\frac{1}{2},L}^n - 1) \end{aligned}$$

Upon differentiating and by (20) it yields

$$\begin{aligned}\frac{\partial K_2}{\partial v_{i-\frac{1}{2},L}^n} &= \frac{\partial H_{i-\frac{1}{2}}^n}{\partial v_{i-\frac{1}{2},L}^n} = -\frac{\lambda \alpha_{i-\frac{1}{2},L}^n}{2} \geq 0 \\ \frac{\partial K_2}{\partial v_{i-\frac{1}{2},L}^n} &= \frac{\partial H_{i-\frac{1}{2}}^n}{\partial v_{i-\frac{1}{2},L}^n} = -\frac{\lambda \alpha_{i-\frac{1}{2},L}^n}{2} \geq 0 \\ \frac{\partial K_2}{\partial v_{i+\frac{1}{2},R}^n} &= \lambda \alpha_{i+\frac{1}{2},R}^n \geq 0 \\ \frac{\partial K_2}{\partial v_{i+\frac{1}{2},L}^n} &= \frac{1}{2} + \Delta t (\alpha_{i+\frac{1}{2},L}^n - 1) \geq 0 \\ \frac{\partial K_2}{\partial v_{i-\frac{1}{2},R}^n} &= \frac{1}{2} - \frac{\lambda \alpha_{i-\frac{1}{2},R}^n}{2} \geq 0\end{aligned}$$

This proves that  $K_2$  is non-decreasing in each of its variables  $v_{i\pm\frac{1}{2},L}^n$  and  $v_{i\pm\frac{1}{2},R}^n$  under the condition (20). Consequently, we obtain  $v_i^{n,*} \geq 0$  as:

$$\begin{aligned}0 &\leq K_2(\alpha_{i-\frac{1}{2},L}^n, \alpha_{i-\frac{1}{2},R}^n, \alpha_{i+\frac{1}{2},L}^n, \alpha_{i+\frac{1}{2},R}^n, v_{i-\frac{1}{2},L}^n, 0, 0, 0) \\ &\leq K_2(\alpha_{i-\frac{1}{2},L}^n, \alpha_{i-\frac{1}{2},R}^n, \alpha_{i+\frac{1}{2},L}^n, \alpha_{i+\frac{1}{2},R}^n, v_{i-\frac{1}{2},L}^n, v_{i-\frac{1}{2},R}^n, v_{i+\frac{1}{2},L}^n, v_{i+\frac{1}{2},R}^n) = v_i^{n,*}\end{aligned}$$

In a similar way and using the fact that  $v_i^{n,*} \geq 0$ , we can show that  $v_i^{n,**} \geq 0$ . Subsequently, through (18), it follows that  $v_i^{n+1} \geq 0$ . This completes the proof of (ii).  $\square$

#### 4 Open table problem in one-dimension and well-balance property

We now show that the the second-order scheme (18) is not well-balanced in general, i.e. the numerical scheme does not capture the steady state solution of (5).

**Theorem 2** *The second-order scheme (18) is well balanced in the state variable  $u$  but not in  $v$ .*

**Proof** Let  $(\bar{u}, \bar{v})$  denote the steady state solution of (6)-(7) (a solution of (5) in one dimension). We take the particular case of  $f \equiv 1$  in  $[0, 1]$ . In this case, the exact steady state solutions are given by

$$(\bar{u}, \bar{v})(x) = \begin{cases} (x, \frac{1}{2} - x) & \text{if } x \in [0, \frac{1}{2}] \\ (1 - x, x - \frac{1}{2}) & \text{if } x \in (\frac{1}{2}, 1] \end{cases} \quad (21)$$

From this we have

$$\bar{\alpha}(x) = \begin{cases} 1 & \text{if } x \in [0, \frac{1}{2}] \\ -1 & \text{if } x \in (\frac{1}{2}, 1] \end{cases}$$

where  $\bar{\alpha} = \bar{u}_x$ . Now, the discrete values of the steady states are given by

$$(\bar{\alpha}_i, \bar{v}_i) = \begin{cases} (1, \frac{1}{2} - x_i), & i \leq K \\ (-1, x_i - \frac{1}{2}), & i > K \end{cases} \quad (22)$$

with  $x_{K+\frac{1}{2}} = 0.5$ . To prove that the scheme is well-balanced in the state variable  $u$  and not in  $v$ , we substitute the discrete form (22) in the second-order scheme as an initial data and show that

$$u_{i+\frac{1}{2}}^1 = u_{i+\frac{1}{2}}^0 = \bar{u}_{i+\frac{1}{2}}, \quad \text{for all } i \in \mathcal{M}$$

and

$$v_i^1 \neq v_i^0 = \bar{v}_i \quad \text{for all } i \in \mathcal{M} \setminus \{0\}$$



where  $\bar{u}_{i+\frac{1}{2}}$  is the discrete value of the steady state  $\bar{u}$  at  $x_{i+\frac{1}{2}}$ . It is important to note that,  $D\alpha_i^0 = 0$  in (13), and consequently we have  $\alpha_{i+\frac{1}{2},L}^0 = \alpha_{i-\frac{1}{2},R}^0 = \alpha_i^0$ . This leads to the simplification:

$$G_{i+\frac{1}{2}}^0 = G(\alpha_{i+\frac{1}{2},L}^0, v_{i+\frac{1}{2},L}^0, \alpha_{i+\frac{1}{2},R}^0, v_{i+\frac{1}{2},R}^0) = 0$$

This gives that  $u_{i+\frac{1}{2}}^{0,*} = u_{i+\frac{1}{2}}^0 = \bar{u}_{i+\frac{1}{2}}$ . Subsequently, we have  $\alpha_i^{0,*} = \alpha_i^0$  and hence  $\alpha_{i+\frac{1}{2},L}^{0,*} = \alpha_{i-\frac{1}{2},R}^{0,*} = \alpha_i^{0,*}$ . This, in turn, implies

$$u_{i+\frac{1}{2}}^{0,**} = u_{i+\frac{1}{2}}^{0,*} = \bar{u}_{i+\frac{1}{2}}$$

and

$$u_{i+\frac{1}{2}}^1 = \frac{1}{2}(u_{i+\frac{1}{2}}^0 + u_{i+\frac{1}{2}}^{0,**}) = \bar{u}_{i+\frac{1}{2}}$$

This shows that the second-order scheme is well-balanced in  $u$ . Now, let us consider the case for  $v$ : note that

$$v_i^0 - v_{i-1}^0 = \begin{cases} -\Delta x, & i \leq K \\ \Delta x, & i \geq K+2 \\ 0, & i = K+1 \end{cases} \quad (23)$$

since  $x_{K+\frac{1}{2}} = \frac{1}{2}$ . From the definition, we have

$$Dv_i^0 = 2\theta \begin{cases} -\Delta x, & i \leq K-1 \\ \Delta x, & i \geq K+2 \\ 0, & i = K, K+1 \end{cases}$$

Now, we compute  $v_i^{0,*}$  from the expression

$$v_i^{0,*} = v_i^0 - \lambda(H_{i+\frac{1}{2}}^0 - H_{i-\frac{1}{2}}^0) + \Delta t S_{i+\frac{1}{2},L}^0 \quad (24)$$

First we observe that  $S_{i+\frac{1}{2},L}^0 = 0$  for all  $i \in \mathcal{M}$  as we have  $|\alpha_{i+\frac{1}{2},L}^0| = 1$ . Now, in the subsequent steps, we calculate the fluxes  $H_{i\pm\frac{1}{2}}^0$  in (24). For this, first we consider the slopes

$$DB_i = 2\theta \text{minmod} \left( B_i - B_{i-1}, \frac{1}{2}(B_{i+1} - B_{i-1}), B_{i+1} - B_i \right)$$

and note that  $DB_i = 2\theta\Delta x$ , as  $B_i = x_i$ . This results in the following values

$$B_{i+\frac{1}{2},L} = x_i + \theta\Delta x \text{ and } B_{i+\frac{1}{2},R} = x_{i+1} - \theta\Delta x$$

Given that

$$\alpha_i^0 = \bar{\alpha}_i^0 = \begin{cases} 1, & i \leq K \\ -1, & i > K \end{cases}$$

we obtain  $\alpha_{i+\frac{1}{2},L}^0 = \alpha_{i-\frac{1}{2},R}^0 = \alpha_i^0$ . Now, using the values  $\alpha_{i+\frac{1}{2},L}^0, \alpha_{i+\frac{1}{2},R}^0, v_{i+\frac{1}{2},L}^0, v_{i+\frac{1}{2},R}^0, B_{i+\frac{1}{2},L}$  and  $B_{i+\frac{1}{2},R}$  in (10), we write the numerical flux as

$$H_{i+\frac{1}{2}}^0 = \begin{cases} v_{i+\frac{1}{2},L}^0 - B_{i+\frac{1}{2},L}, & i \geq K+1 \\ -v_{i+\frac{1}{2},R}^0 - B_{i+\frac{1}{2},R}, & i \leq K-1 \\ -\frac{1}{2}(B_{i+\frac{1}{2},L} + B_{i+\frac{1}{2},R}), & i = K \end{cases}$$

$$= \begin{cases} v_i^0 + \frac{1}{2}Dv_i^0 - x_i - \theta\Delta x, & i \geq K+1 \\ -v_{i+1}^0 + \frac{1}{2}Dv_{i+1}^0 - x_{i+1} + \theta\Delta x, & i \leq K-1 \\ -\frac{1}{2}(x_i + x_{i+1}), & i = K \end{cases}$$

which reduces to

$$H_{i+\frac{1}{2}}^0 = -\frac{1}{2} + \theta \begin{cases} 0, & i \geq K+2 \\ -\Delta x, & i = K+1 \\ 2\Delta x, & i \leq K-2 \\ \Delta x, & i = K-1 \\ 0, & i = K \end{cases}$$

By calculating the difference of the fluxes

$$H_{i+\frac{1}{2}}^0 - H_{i-\frac{1}{2}}^0 = \theta \begin{cases} 0, & i \geq K+3, i \leq K-2 \\ \Delta x, & i = K+2 \\ -\Delta x, & K-1 \leq i \leq K+1 \end{cases}$$

and inserting in (24), it yields

$$v_i^{0,*} = v_i^0 + \theta \begin{cases} 0, & i \geq K+3, i \leq K-2 \\ -\Delta t, & i = K+2 \\ \Delta t, & K-1 \leq i \leq K+1 \end{cases} \quad (25)$$

Now, to compute  $v_i^{0,**}$ , we need the following slopes

$$Dv_i^{0,*} = 2\theta \min\text{mod} \left( v_i^{0,*} - v_{i-1}^{0,*}, \frac{1}{2}(v_{i+1}^{0,*} - v_{i-1}^{0,*}), v_{i+1}^{0,*} - v_i^{0,*} \right)$$

By using (25) and (23), we have

$$Dv_i^{0,*} = 2\theta \begin{cases} \min\text{mod} \left( \Delta x + \theta\Delta t, \frac{1}{2}(2\Delta x + \theta\Delta t), \Delta x \right), & i = K+3 \\ \min\text{mod} \left( -\Delta x, \frac{1}{2}(\theta\Delta t - 2\Delta x), -\Delta x + \theta\Delta t \right), & i = K-2 \\ \Delta x, & i \geq K+4 \\ -\Delta x, & i \leq K-3 \\ 2\theta \min\text{mod} \left( -\Delta x + \Delta t\theta, \frac{1}{2}(\theta\Delta t - 2\Delta x), -\Delta x \right), & i = K-1 \\ \min\text{mod} \left( \Delta x - 2\theta\Delta t, \Delta x - \frac{1}{2}\theta\Delta t, \Delta x + \theta\Delta t \right), & i = K+2 \\ 0, & i = K, K+1 \end{cases}$$

$$= 2\theta \begin{cases} \Delta x, & i \geq K+3 \\ \Delta x - 2\theta\Delta t, & i = K+2 \\ 0, & i = K, K+1 \\ -\Delta x + \theta\Delta t, & i = K-1, K-2 \\ -\Delta x, & i \leq K-3 \end{cases}$$

Using this values, we compute  $v_{i+\frac{1}{2},L}^{0,*}$  and  $v_{i+\frac{1}{2},R}^{0,*}$  and there by obtain the flux  $H_{i+\frac{1}{2}}^{0,*}$  ( by (10) ) as

$$H_{i+\frac{1}{2}}^{0,*} = \begin{cases} v_{i+\frac{1}{2},L}^{0,*} - B_{i+\frac{1}{2},L}, & i \geq K+1 \\ -v_{i+\frac{1}{2},R}^{0,*} - B_{i+\frac{1}{2},R}, & i \leq K-1 \\ -\frac{1}{2}(B_{i+\frac{1}{2},L} + B_{i+\frac{1}{2},R}), & i = K \end{cases}$$

$$= \begin{cases} v_i^{0,*} + \frac{1}{2}Dv_i^{0,*} - x_i - \theta\Delta x, & i \geq K+1 \\ -v_{i+1}^{0,*} + \frac{1}{2}Dv_{i+1}^{0,*} - x_{i+1} + \theta\Delta x, & i \leq K-1 \\ -\frac{1}{2}(x_i + x_{i+1}), & i = K \end{cases}$$

By substituting the value of  $v_i^{0,*}$  from (25) in the above expression, we get

$$H_{i+\frac{1}{2}}^{0,*} = \begin{cases} v_i^0 + \theta\Delta t - x_i - \theta\Delta x, & i = K+1 \\ v_i^0 - \theta\Delta t + \theta\Delta x - 2\theta^2\Delta t - x_i - \theta\Delta x, & i = K+2 \\ v_i^0 + \theta\Delta x - x_i - \theta\Delta x, & i \geq K+3 \\ -v_K^0 - \theta\Delta t - x_{i+1} + \theta\Delta x, & i = K-1 \\ -v_{K-1}^0 - \theta\Delta t - \theta\Delta x + \theta^2\Delta t - x_{i+1} + \theta\Delta x, & i = K-2 \\ -v_{K-2}^0 - \theta\Delta x + \theta^2\Delta t - x_{i+1} + \theta\Delta x, & i = K-3 \\ -v_{i+1}^0 - \theta\Delta x - x_{i+1} + \theta\Delta x, & i \leq K-4 \\ -\frac{1}{2}, & i = K \end{cases}$$

Now, taking the flux difference, we arrive at:

$$H_{i+\frac{1}{2}}^{0,*} - H_{i-\frac{1}{2}}^{0,*} = \theta \begin{cases} \Delta t - \Delta x, & i = K + 1 \\ -2\Delta t - 2\theta\Delta t + \Delta x, & i = K + 2 \\ \Delta t + 2\theta\Delta x, & i \geq K + 3 \\ \Delta x - \theta\Delta t, & i = K - 1 \\ -\Delta t, & i = K - 2 \\ \theta\Delta t, & i = K - 3 \\ 0, & i \leq K - 4 \\ \Delta t - \Delta x, & i = K \end{cases}$$

Finally, we get

$$v_i^{0,**} = v_i^{0,*} - \lambda\theta \begin{cases} \Delta t - \Delta x, & i = K + 1 \\ -2\Delta t - 2\theta\Delta t + \Delta x, & i = K + 2 \\ \Delta t + 2\theta\Delta x, & i \geq K + 3 \\ \Delta x - \theta\Delta t, & i = K - 1 \\ -\Delta t, & i = K - 2 \\ \theta\Delta t, & i = K - 3 \\ 0, & i \leq K - 4 \\ \Delta t - \Delta x, & i = K \end{cases}$$

Once again using the value of  $v_i^{0,*}$  from (25) in the above expression, we deduce that

$$v_i^{0,**} = v_i^0 + \theta \begin{cases} \Delta t - \lambda(\Delta t - \Delta x), & i = K + 1 \\ -\Delta t - \lambda(-2\Delta t - 2\theta\Delta t + \Delta x), & i = K + 2 \\ -\lambda(\Delta t + 2\theta\Delta x), & i \geq K + 3 \\ +\Delta t - \lambda(\Delta x - \theta\Delta t), & i = K - 1 \\ -\lambda(-\Delta t), & i = K - 2 \\ -\lambda(\theta\Delta t), & i = K - 3 \\ 0, & i \leq K - 4 \\ \Delta t - \lambda(\Delta t - \Delta x), & i = K \end{cases}$$

Noting that the solution  $v$  at the single time step is given by

$$v_i^1 = \frac{1}{2}(v_i^0 + v_i^{0,**})$$

we finally arrive at:

$$v_i^1 = v_i^0 + \frac{\theta}{2} \begin{cases} \Delta t - \lambda(\Delta t - \Delta x), & i = K + 1 \\ -\Delta t - \lambda(-2\Delta t - 2\theta\Delta t + \Delta x), & i = K + 2 \\ -\lambda(\Delta t + 2\theta\Delta x), & i \geq K + 3 \\ \Delta t - \lambda(\Delta x - \theta\Delta t), & i = K - 1 \\ -\lambda(-\Delta t), & i = K - 2 \\ -\lambda(\theta\Delta t), & i = K - 3 \\ 0, & i \leq K - 4 \\ \Delta t - \lambda(\Delta t - \Delta x), & i = K \end{cases}$$

This shows that the second-order scheme (18) is not well balanced for  $\theta \neq 0$ . □

## 5 Second-order adaptive scheme in one-dimension

To produce a well-balanced second-order scheme, we propose a modification to the second-order scheme (18) based on the idea introduced in [19, 23, 31]. The main principle involves using the the second-order scheme (18) away from the steady states and reducing it to the first-order scheme (8) near the steady states. This modification results in a

second-order scheme that is well-balanced. The measure of the closeness to a steady state is determined through the following procedure. We define a smooth function  $\Theta$  such that

$$\Theta(x) := \frac{x^2}{x^2 + \Delta x^2}, \quad x \in \mathbb{R}. \quad (26)$$

Note that  $\Theta(0) = 0$  and  $\Theta(x) \approx 1$  for  $x \neq 0$  and sufficiently small  $\Delta x$ . For each  $(i, n) \in (\mathcal{M} \setminus \{0\}) \times \mathcal{N}_T$ , we define

$$\begin{aligned} \Theta_i^n &:= \Theta(\mathcal{E}_i^n) \\ \mathcal{E}_i^n &:= \mathcal{E}_{i-\frac{1}{2}}^n + \mathcal{E}_{i+\frac{1}{2}}^n \\ \mathcal{E}_{i+\frac{1}{2}}^n &:= \sqrt{(G_{i+\frac{1}{2}}^n)^2 + [H_{i+\frac{1}{2}}^n]^2} \end{aligned} \quad (27)$$

where

$$\begin{aligned} [H_{i+\frac{1}{2}}^n] &:= H_{i+\frac{1}{2}}^n - H_{i-\frac{1}{2}}^n \\ H_{i+\frac{1}{2}}^n &= H(\alpha_i^n, v_i^n, \alpha_{i+1}^n, v_{i+1}^n, B_i, B_{i+1}) \\ G_{i+\frac{1}{2}}^n &= G(\alpha_i^n, v_i^n, \alpha_{i+1}^n, v_{i+1}^n) \end{aligned}$$

Here,  $G$  and  $H$  are given by (9) and (10), respectively. In each Runge-Kutta stage, previously defined left and right states (15) are modified for the linear function  $z = \alpha, v$  and  $B$  in  $[x_{i-\frac{1}{2}}, x_{i+\frac{1}{2}}]$  as follows:

$$z_{i+\frac{1}{2},L}^n = z_i^n + \frac{1}{2}\Theta_i^n D z_i^n, \quad z_{i-\frac{1}{2},R}^n = z_i^n - \frac{1}{2}\Theta_i^n D z_i^n \quad (28)$$

$$z_{i+\frac{1}{2},L}^{n,*} = z_i^{n,*} + \frac{1}{2}\Theta_i^n D z_i^{n,*}, \quad z_{i-\frac{1}{2},R}^{n,*} = z_i^{n,*} - \frac{1}{2}\Theta_i^n D z_i^{n,*} \quad (29)$$

where  $D z_i^n, D z_i^{n,*}$  are defined as before in Section 2. Using these modified values (28) and (29), we compute  $u_{i+\frac{1}{2}}^{n,*}, u_{i+\frac{1}{2}}^{n,**}, v_i^{n,*}$  and  $v_i^{n,**}$ . The resulting adaptive second-order scheme is now expressed as

$$\begin{aligned} u_{i+\frac{1}{2}}^{n+1} &= \frac{1}{2}(u_{i+\frac{1}{2}}^n + u_{i+\frac{1}{2}}^{n,**}) \\ v_i^{n+1} &= \frac{1}{2}(v_i^n + v_i^{n,**}) \end{aligned} \quad (30)$$

**Theorem 3** *The adaptive scheme (30) is well-balanced and second-order accurate away from the steady state.*

**Proof** To prove that the scheme is well-balanced, it suffices to show that

$$(u_{i+\frac{1}{2}}^1, v_i^1) = (u_{i+\frac{1}{2}}^0, v_i^0) = (\bar{u}_{i+\frac{1}{2}}, \bar{v}_i)$$

where  $(\bar{u}_{i+\frac{1}{2}}, \bar{v}_i)$  are the discrete steady states, as given in the proof of Theorem 2. As the first-order scheme is well-balanced (see [3]), it follows that  $\Theta_i^0 = 0$ . Consequently, in the RK step-1 of the adaptive scheme (30), we obtain

$$u_{i+\frac{1}{2}}^{0,*} = u_{i+\frac{1}{2}}^0 = \bar{u}_{i+\frac{1}{2}}, \quad v_i^{0,*} = v_i^0 = \bar{v}_i \text{ and } \alpha_i^{0,*} = \alpha_i^0 = \bar{\alpha}_i$$

Similarly, in the RK step-2, we obtain,

$$u_{i+\frac{1}{2}}^{0,**} = \bar{u}_{i+\frac{1}{2}} \text{ and } v_i^{0,**} = \bar{v}_i$$

Therefore, from the adaptive scheme (30), we get  $u_{i+\frac{1}{2}}^1 = \bar{u}_{i+\frac{1}{2}}$  and  $v_i^1 = \bar{v}_i$ . Further, we observe that  $\mathcal{E}_i^0 \neq 0$  away from the steady state, leading to the fact that  $\Theta_i^0 \approx 1$  for sufficiently small  $\Delta x$  (see [19, 23, 31]). This shows that the adaptive scheme (30) is second-order accurate away from the steady state.  $\square$

## 6 Numerical schemes in two-dimensions

In this section, we extend the scheme constructed in the previous sections to the two dimensional case. The system of equations in two dimensions is written as

$$u_t + (\sqrt{u_x^2 + u_y^2} - 1)v = 0, \quad \text{in } \Omega \times (0, T] \quad (31)$$

$$v_t + (-u_x v - B^x)_x + (-u_y v - B^y)_y - (\sqrt{u_x^2 + u_y^2} - 1)v = 0, \quad \text{in } \Omega \times (0, T] \quad (32)$$

$$u(x, y, 0) = v(x, y, 0) = 0, \quad \text{in } \Omega$$

where  $B^x = B^x(x, y) = \int_0^x f_1(\xi, y) d\xi$ ,  $B^y(x, y) = \int_0^y f_2(x, \xi) d\xi$  with  $f_1$  and  $f_2$  are such that  $f = f_1 + f_2$ . The splitting of the source term  $f$  will be explained later. The system (31)-(32) is solved with boundary conditions as given in (4).

We consider the domain  $\Omega = (0, 1) \times (0, 1)$ . Define the space grid points along x-axis as  $x_{i+\frac{1}{2}} = i\Delta x$ ,  $\Delta x > 0$ ,  $i \in \mathcal{M}$  and along y-axis as  $y_{k+\frac{1}{2}} = k\Delta y$ ,  $\Delta y > 0$ ,  $k \in \mathcal{M}$  with  $(x_{\frac{1}{2}}, y_{\frac{1}{2}}) = (0, 0)$  and  $(x_{M+\frac{1}{2}}, y_{M+\frac{1}{2}}) = (1, 1)$ . For simplicity, we set  $\Delta x = \Delta y = h$  and for  $\Delta t > 0$ , define the time discretization points  $t^n = n\Delta t$ ,  $n \in \mathcal{N}_T$  with  $\lambda = \Delta t/h$ . The numerical approximation of  $u$  at the point  $(x_{i+\frac{1}{2}}, y_{k+\frac{1}{2}})$ ,  $i, k \in \mathcal{M}$  at time  $t^n$  is denoted by  $u_{i+\frac{1}{2}, k+\frac{1}{2}}^n$ . For  $i, k \in \mathcal{M} \setminus \{0\}$ , the solution  $v$  in the cell  $C_{i,k}$  at time  $t^n$  is given by

$$v_{i,k}^n = \frac{1}{h^2} \int_{C_{i,k}} v(x, y, t^n) dx dy.$$

A pictorial illustration of the grid  $C_{i,k}$  is given in Fig 1, where we suppress the time index  $n$  for simplicity.

## 6.1 Second-order scheme

Similar to the one-dimensional case, we derive a second-order scheme in two dimensions by employing a MUSCL type spatial reconstruction in space and strong stability preserving Runge-Kutta method in time. To begin with, let  $\alpha := u_x$  and  $\beta := u_y$ , and define their approximations as follows:

$$\alpha_{i,k+\frac{1}{2}}^n = \frac{u_{i+\frac{1}{2}, k+\frac{1}{2}}^n - u_{i-\frac{1}{2}, k+\frac{1}{2}}^n}{h}, \quad i \in \mathcal{M} \setminus \{0\}, k \in \mathcal{M}$$

$$\beta_{i+\frac{1}{2}, k}^n = \frac{u_{i+\frac{1}{2}, k+\frac{1}{2}}^n - u_{i+\frac{1}{2}, k-\frac{1}{2}}^n}{h}, \quad k \in \mathcal{M} \setminus \{0\}, i \in \mathcal{M}$$

Next, we define the slopes corresponding to grid points  $i + \frac{1}{2}$  and  $k + \frac{1}{2}$  as

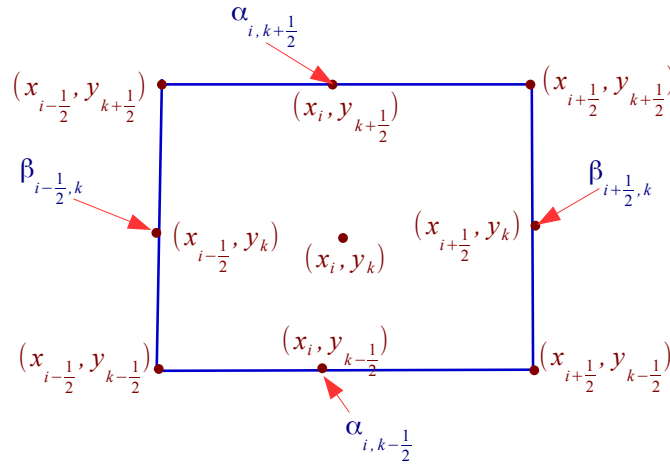


Figure 1: An element  $C_{i,k}$  of the two dimensional Cartesian grids

$$D\alpha_{i,k+\frac{1}{2}}^n = 2\theta \min\text{mod} \left( \alpha_{i+1, k+\frac{1}{2}}^n - \alpha_{i, k+\frac{1}{2}}^n, \frac{1}{2}(\alpha_{i+1, k+\frac{1}{2}}^n - \alpha_{i-1, k+\frac{1}{2}}^n), \alpha_{i, k+\frac{1}{2}}^n - \alpha_{i-1, k+\frac{1}{2}}^n \right)$$

for  $i \in \mathcal{M} \setminus \{0\}$ ,  $k \in \mathcal{M}$  and

$$D\beta_{i+\frac{1}{2},k}^n = 2\theta \min\text{mod} \left( \beta_{i+\frac{1}{2},k+1}^n - \beta_{i+\frac{1}{2},k}^n, \frac{1}{2}(\beta_{i+\frac{1}{2},k+1}^n - \beta_{i+\frac{1}{2},k}^n), \beta_{i+\frac{1}{2},k}^n - \beta_{i+\frac{1}{2},k-1}^n \right)$$

for  $k \in \mathcal{M} \setminus \{0\}$ ,  $i \in \mathcal{M}$ . Using this, we reconstruct piecewise linear functions with left and right end point values

$$\begin{aligned} \alpha_{i+\frac{1}{2},L,k+\frac{1}{2}}^n &= \alpha_{i,k+\frac{1}{2}}^n + \frac{1}{2}D\alpha_{i,k+\frac{1}{2}}^n, & \alpha_{i-\frac{1}{2},R,k+\frac{1}{2}}^n &= \alpha_{i,k+\frac{1}{2}}^n - \frac{1}{2}D\alpha_{i,k+\frac{1}{2}}^n \\ \beta_{i+\frac{1}{2},k+\frac{1}{2},L}^n &= \beta_{i+\frac{1}{2},k}^n + \frac{1}{2}D\beta_{i+\frac{1}{2},k}^n, & \beta_{i+\frac{1}{2},k-\frac{1}{2},R}^n &= \beta_{i+\frac{1}{2},k}^n - \frac{1}{2}D\beta_{i+\frac{1}{2},k}^n \end{aligned}$$

Now, we detail the linear reconstruction of  $v$  using the minmod limiter in  $x$  and  $y$  direction. For the given values  $v_{i,k}^n$  in the cell  $[x_{i-\frac{1}{2}}, x_{i+\frac{1}{2}}] \times [y_{k-\frac{1}{2}}, y_{k+\frac{1}{2}}]$ , define the slopes as

$$\begin{aligned} Dv_{i,k}^{n,x} &= 2\theta \min\text{mod} \left( v_{i+1,k}^n - v_{i,k}^n, \frac{1}{2}(v_{i+1,k}^n - v_{i-1,k}^n)v_{i,k}^n - v_{i-1,k}^n \right) \\ Dv_{i,k}^{n,y} &= 2\theta \min\text{mod} \left( v_{i,k+1}^n - v_{i,k}^n, \frac{1}{2}(v_{i,k+1}^n - v_{i,k-1}^n)v_{i,k}^n - v_{i,k-1}^n \right) \end{aligned}$$

and obtain the left and right values

$$\begin{aligned} v_{i+\frac{1}{2},L,k}^n &= v_{i,k}^n + \frac{1}{2}Dv_{i,k}^{n,x}, & v_{i-\frac{1}{2},R,k}^n &= v_{i,k}^n - \frac{1}{2}Dv_{i,k}^{n,x} \\ v_{i,k+\frac{1}{2},L}^n &= v_{i,k}^n + \frac{1}{2}Dv_{i,k}^{n,y}, & v_{i,k-\frac{1}{2},R}^n &= v_{i,k}^n - \frac{1}{2}Dv_{i,k}^{n,y} \end{aligned} \tag{33}$$

$$\begin{aligned} v_{i+\frac{1}{2},L,k+\frac{1}{2}}^n &= \frac{v_{i+\frac{1}{2},L,k}^n + v_{i+\frac{1}{2},L,k+1}^n}{2}, & v_{i+\frac{1}{2},R,k+\frac{1}{2}}^n &= \frac{v_{i+\frac{1}{2},R,k}^n + v_{i+\frac{1}{2},R,k+1}^n}{2} \\ v_{i+\frac{1}{2},k+\frac{1}{2},L}^n &= \frac{v_{i,k+\frac{1}{2},L}^n + v_{i+1,k+\frac{1}{2},L}^n}{2}, & v_{i+\frac{1}{2},k+\frac{1}{2},R}^n &= \frac{v_{i,k+\frac{1}{2},R}^n + v_{i+1,k+\frac{1}{2},R}^n}{2} \end{aligned}$$

Note that in the  $y$  direction, left and right values correspond to the values from the bottom and the top, respectively. Now, using this reconstructed values, we write the numerical fluxes at the  $n$  th time step in the following lines. First, we write the approximation for  $u_x$  and  $u_y$  as

$$\begin{aligned} (u_x)^2 &\approx \tilde{G}_{i+\frac{1}{2},k+\frac{1}{2}}^{n,x} = \left( \max(|\max(\alpha_{i+\frac{1}{2},L,k+\frac{1}{2}}^n, 0)|, |\min(\alpha_{i+\frac{1}{2},R,k+\frac{1}{2}}^n, 0)|) \right)^2 \\ (u_y)^2 &\approx \tilde{G}_{i+\frac{1}{2},k+\frac{1}{2}}^{n,y} = \left( \max(|\max(\beta_{i+\frac{1}{2},k+\frac{1}{2},L}^n, 0)|, |\min(\beta_{i+\frac{1}{2},k+\frac{1}{2},R}^n, 0)|) \right)^2 \end{aligned}$$

Define

$$\begin{aligned} W_{i,k+\frac{1}{2}}^{n,x} &= \left( \sqrt{(|\max(\alpha_{i+\frac{1}{2},L,k+\frac{1}{2}}^n, 0)|)^2 + \tilde{G}_{i+\frac{1}{2},k+\frac{1}{2}}^{n,y}} - 1 \right) v_{i+\frac{1}{2},L,k+\frac{1}{2}}^n \\ W_{i+1,k+\frac{1}{2}}^{n,x} &= \left( \sqrt{|\min(\alpha_{i+\frac{1}{2},R,k+\frac{1}{2}}^n, 0)|^2 + \tilde{G}_{i+\frac{1}{2},k+\frac{1}{2}}^{n,y}} - 1 \right) v_{i+\frac{1}{2},R,k+\frac{1}{2}}^n \\ W_{i+\frac{1}{2},k}^{n,y} &= \left( \sqrt{|\max(\beta_{i+\frac{1}{2},k+\frac{1}{2},L}^n, 0)|^2 + \tilde{G}_{i+\frac{1}{2},k+\frac{1}{2}}^{n,x}} - 1 \right) v_{i+\frac{1}{2},k+\frac{1}{2},L}^n \\ W_{i+\frac{1}{2},k+1}^{n,y} &= \left( \sqrt{|\min(\beta_{i+\frac{1}{2},k+\frac{1}{2},R}^n, 0)|^2 + \tilde{G}_{i+\frac{1}{2},k+\frac{1}{2}}^{n,x}} - 1 \right) v_{i+\frac{1}{2},k+\frac{1}{2},R}^n \end{aligned}$$

Now, the numerical fluxes in the  $x$  and  $y$ - directions are given by

$$G_{i+\frac{1}{2},k+\frac{1}{2}}^{n,x} = \max(W_{i,k+\frac{1}{2}}^{n,x}, W_{i+1,k+\frac{1}{2}}^{n,x}) \text{ and } G_{i+\frac{1}{2},k+\frac{1}{2}}^{n,y} = \max(W_{i+\frac{1}{2},k}^{n,y}, W_{i+\frac{1}{2},k+1}^{n,y})$$

respectively. Finally, we write the term

$$\begin{aligned} G_{i+\frac{1}{2},k+\frac{1}{2}}^n &= \max(G_{i+\frac{1}{2},k+\frac{1}{2}}^{n,x}, G_{i+\frac{1}{2},k+\frac{1}{2}}^{n,y}) \\ &= G(\alpha_{i+\frac{1}{2},L,k+\frac{1}{2}}^n, \alpha_{i+\frac{1}{2},R,k+\frac{1}{2}}^n, \beta_{i+\frac{1}{2},k+\frac{1}{2},L}^n, \beta_{i+\frac{1}{2},k+\frac{1}{2},R}^n, \\ &\quad v_{i+\frac{1}{2},L,k+\frac{1}{2}}^n, v_{i+\frac{1}{2},R,k+\frac{1}{2}}^n, v_{i+\frac{1}{2},k+\frac{1}{2},L}^n, v_{i+\frac{1}{2},k+\frac{1}{2},R}^n) \end{aligned} \tag{34}$$

which approximates

$$G(u, v) = (\sqrt{(u_x^2 + u_y^2) - 1})v$$

at  $(x_{i+\frac{1}{2}}, y_{k+\frac{1}{2}})$  and  $t^n$ . For the approximation of  $v$ , we consider the following flux functions at the  $n$  th stage:

$$\begin{aligned} H_{i+\frac{1}{2},k}^{n,x} &= H(\alpha_{i+\frac{1}{2},L,k}^n, \alpha_{i+\frac{1}{2},R,k}^n, v_{i+\frac{1}{2},L,k}^n, v_{i+\frac{1}{2},R,k}^n, B_{i+\frac{1}{2},L,k}^x, B_{i+\frac{1}{2},R,k}^x) \\ H_{i,k+\frac{1}{2}}^{n,y} &= H(\beta_{i,k+\frac{1}{2},L}^n, \beta_{i,k+\frac{1}{2},R}^n, v_{i,k+\frac{1}{2},L}^n, v_{i,k+\frac{1}{2},R}^n, B_{i,k+\frac{1}{2},L}^y, B_{i,k+\frac{1}{2},R}^y) \end{aligned} \quad (35)$$

with

$$\begin{aligned} \alpha_{i+\frac{1}{2},L,k}^n &= \alpha_{i,k}^n + \frac{1}{2}D\alpha_{i,k}^n \\ \alpha_{i-\frac{1}{2},R,k}^n &= \alpha_{i,k}^n - \frac{1}{2}D\alpha_{i,k}^n \\ \beta_{i,k+\frac{1}{2},L}^n &= \beta_{i,k}^n + \frac{1}{2}D\beta_{i,k}^n \\ \beta_{i,k-\frac{1}{2},R}^n &= \beta_{i,k}^n - \frac{1}{2}D\beta_{i,k}^n \end{aligned}$$

where the slopes are given by

$$\begin{aligned} D\alpha_{i,k}^n &= 2\theta \min\text{mod} \left( \alpha_{i+1,k}^n - \alpha_{i,k}^n, \frac{1}{2}(\alpha_{i+1,k}^n - \alpha_{i-1,k}^n), \alpha_{i,k}^n - \alpha_{i-1,k}^n \right) \\ D\beta_{i,k}^n &= 2\theta \min\text{mod} \left( \beta_{i,k+1}^n - \beta_{i,k}^n, \frac{1}{2}(\beta_{i,k+1}^n - \beta_{i,k-1}^n), \beta_{i,k}^n - \beta_{i,k-1}^n \right) \end{aligned}$$

and  $\alpha_{i,k}^n, \beta_{i,k}^n$  are computed as

$$\alpha_{i,k}^n = \frac{1}{2}(\alpha_{i,k+\frac{1}{2}}^n + \alpha_{i,k-\frac{1}{2}}^n) \text{ and } \beta_{i,k}^n = \frac{1}{2}(\beta_{i+\frac{1}{2},k}^n + \beta_{i-\frac{1}{2},k}^n)$$

Further, the values  $v_{i+\frac{1}{2},L,k}^n, v_{i+\frac{1}{2},R,k}^n, v_{i,k+\frac{1}{2},L}^n, v_{i,k+\frac{1}{2},R}^n$  are taken as in (33). The terms  $B_{i+\frac{1}{2},L,k}^x, B_{i+\frac{1}{2},R,k}^x$  and  $B_{i,k+\frac{1}{2},L}^y, B_{i,k+\frac{1}{2},R}^y$  are the approximations of  $B^x$  and  $B^y$ , respectively and are given in Section 6.3. Using the terms (34) and fluxes in (35), we compute the approximations  $u_{i+\frac{1}{2},k+\frac{1}{2}}^{n,*}$  and  $v_{i,k}^{n,*}$  in the RK Step-1 as

$$\begin{aligned} u_{i+\frac{1}{2},k+\frac{1}{2}}^{n,*} &= u_{i+\frac{1}{2},k+\frac{1}{2}}^n - \Delta t G_{i+\frac{1}{2},k+\frac{1}{2}}^n, \\ v_{i,k}^{n,*} &= v_{i,k}^n - \lambda (H_{i+\frac{1}{2},k}^{n,x} - H_{i-\frac{1}{2},k}^{n,x}) - \lambda (H_{i,k+\frac{1}{2}}^{n,y} - H_{i,k-\frac{1}{2}}^{n,y}) \\ &\quad + \Delta t (\sqrt{(\alpha_{i+\frac{1}{2},L,k}^n)^2 + (\beta_{i,k+\frac{1}{2},L}^n)^2 - 1}) v_{i,k}^n \end{aligned}$$

We compute the values  $u_{i+\frac{1}{2},k+\frac{1}{2}}^{n,**}$  and  $v_{i,k}^{n,**}$  in the RK Step-2 stage analogously to the one-dimensional case. Finally, the second-order scheme for (1) in two-dimensions is given by

$$\begin{aligned} u_{i+\frac{1}{2},k+\frac{1}{2}}^{n+1} &= \frac{1}{2}(u_{i+\frac{1}{2},k+\frac{1}{2}}^n + u_{i+\frac{1}{2},k+\frac{1}{2}}^{n,**}) \\ v_{i,k}^{n+1} &= \frac{1}{2}(v_{i,k}^n + v_{i,k}^{n,**}) \end{aligned} \quad (36)$$

## 6.2 Second-order adaptive scheme

Similar to the one-dimensional case, we now use the adaptation procedure on the second-order scheme (36) to ensure the well-balance property. Now, define

$$\mathcal{E}_{i+\frac{1}{2},k+\frac{1}{2}}^n := \sqrt{[H_{i+\frac{1}{2},k}^{n,x}] + [H_{i,k+\frac{1}{2}}^{n,y}]^2 + (G_{i+\frac{1}{2},k+\frac{1}{2}}^n)^2}$$

where

$$\begin{aligned} [H_{i+\frac{1}{2},k}^{n,x}] &:= H_{i+\frac{1}{2},k}^{n,x} - H_{i-\frac{1}{2},k}^{n,x} \\ [H_{i,k+\frac{1}{2}}^{n,y}] &:= H_{i,k+\frac{1}{2}}^{n,y} - H_{i,k-\frac{1}{2}}^{n,y} \end{aligned}$$

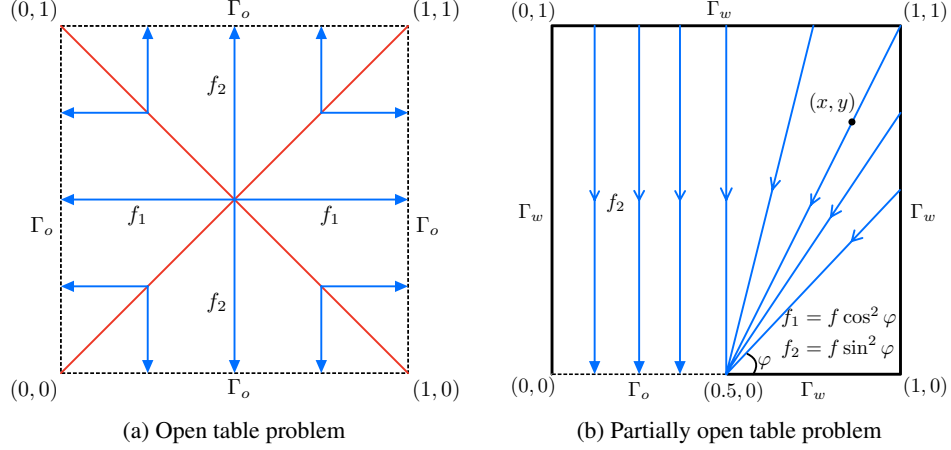


Figure 2: The domain  $\Omega$  and the boundary  $\Gamma$  with transport rays.

with the fluxes  $G_{i+\frac{1}{2},k+\frac{1}{2}}^n$ ,  $H_{i+\frac{1}{2},k}^{n,x}$  and  $H_{i+\frac{1}{2},k}^{n,y}$  are given by

$$\begin{aligned} G_{i+\frac{1}{2},k+\frac{1}{2}}^n &= G(\alpha_{i,k+\frac{1}{2}}^n, \alpha_{i+1,k+\frac{1}{2}}^n, \beta_{i+\frac{1}{2},k}^n, \beta_{i+\frac{1}{2},k+1}^n, v_{i,k+\frac{1}{2}}^n, v_{i+1,k+\frac{1}{2}}^n, v_{i+\frac{1}{2},k}^n, v_{i+\frac{1}{2},k+1}^n) \\ H_{i+\frac{1}{2},k}^{n,x} &= H(\alpha_{i,k}^n, \alpha_{i+1,k}^n, v_{i,k}^n, v_{i+1,k}^n, B_{i,k}^x, B_{i+1,k}^x) \\ H_{i,k+\frac{1}{2}}^{n,y} &= H(\beta_{i,k}^n, \beta_{i,k+1}^n, v_{i,k}^n, v_{i,k+1}^n, B_{i,k}^y, B_{i,k+1}^y) \end{aligned}$$

where  $G$  and  $H$  are computed as in (34) and (35), respectively. Further, define the steady state indicator in each cell as

$$\Theta_{i,k}^n := n\Theta_{i,k}^{n,x} + \Theta_{i,k}^{n,y}$$

where

$$\Theta_{i,k}^{n,x} := \Theta(\mathcal{E}_{i,k+\frac{1}{2}}^n), \quad \mathcal{E}_{i,k+\frac{1}{2}}^n = \mathcal{E}_{i-\frac{1}{2},k+\frac{1}{2}}^n + \mathcal{E}_{i+\frac{1}{2},k+\frac{1}{2}}^n$$

and

$$\Theta_{i,k}^{n,y} := \Theta(\mathcal{E}_{i+\frac{1}{2},k}^n), \quad \mathcal{E}_{i+\frac{1}{2},k}^n = \mathcal{E}_{i+\frac{1}{2},k-\frac{1}{2}}^n + \mathcal{E}_{i+\frac{1}{2},k+\frac{1}{2}}^n$$

The function  $\Theta$  is as defined in (26). Finally, the adaptive second-order scheme is derived by modifying the slopes using  $\Theta_{i,k}^n$  following a similar approach as in the one dimensional case.

### 6.3 Computation of the terms $B^x$ and $B^y$ in two dimensions

The computation of the terms  $B^x$  and  $B^y$  is as given in [1, 3]. For completeness, we briefly review the construction in this section. Absorbing the source term with the convection terms is done by decomposing the source function  $f$  using the concept of *Transport Rays* (blue lines in Fig. 2). This yields better results at the steady states, see [1, 3]. The terms  $B^x$  and  $B^y$  are defined as

$$B^x(x, y) = \int_0^x f_1(\xi, y) d\xi \quad \forall y \in [0, 1], \quad B^y(x, y) = \int_0^y f_2(x, \xi) d\xi \quad \forall x \in [0, 1]$$

where  $f_1$  and  $f_2$  have to be chosen appropriately such that the source term  $f = f_1 + f_2$ . The splitting is given as

$$f_1 = f \cos^2 \varphi, \quad f_2 = f \sin^2 \varphi \quad (37)$$

where  $\varphi$  is the angle which the transport ray  $R_{(x,y)}$  makes with the positive  $x$ -axis. In the case of open table problem, the transport rays are as given in Fig. 2 (a) and the functions  $f_1$  and  $f_2$  are determined as

$$f_1(x, y) = \begin{cases} f(x, y) & \text{if } \{x \geq y, x + y \geq 1\} \cup \{x \leq y, x + y \leq 1\} \\ 0 & \text{otherwise} \end{cases} \quad (38)$$



and

$$f_2(x, y) = \begin{cases} f(x, y) & \text{if } \{x \geq y, x + y \leq 1\} \cup \{x \leq y, x + y \geq 1\} \\ 0 & \text{otherwise} \end{cases} \quad (39)$$

For more details, refer to [3]. In the case of partially open table problem, illustrated in Fig. 2 (b), the angle is computed as  $\varphi = \tan^{-1}(\frac{y}{x-\frac{1}{2}})$ , and the functions  $f_1$  and  $f_2$  are computed as in (37). The numerical approximation of  $B^x$  and  $B^y$  are given by

$$B_{i,k}^x = \int_0^{x_i} f_1(\xi, y_k) d\xi, \quad B_{i,k}^y = \int_0^{y_k} f_2(x_i, \xi) d\xi \quad (40)$$

and to approximate these integrals, we use composite trapezoidal rule. For more details, see [1].

#### 6.4 Boundary conditions

Here, we consider two types of problems similar to the one dimensional case.

**Case 1** (open table problem): in this case, for computing the  $u$  variable, we impose the boundary conditions by setting

$$\begin{aligned} u_{\frac{1}{2}, k+\frac{1}{2}}^n &= u_{M+\frac{1}{2}, k+\frac{1}{2}}^n = 0 \\ u_{i+\frac{1}{2}, \frac{1}{2}}^n &= u_{i+\frac{1}{2}, M+\frac{1}{2}}^n = 0, \quad i, k \in \mathcal{M} \end{aligned}$$

Moreover, to compute the fluxes at the interior vertices of the boundary cells, we need the slopes in the boundary cells. For simplicity, we set these slopes to zero. The boundary conditions for  $v$  are prescribed through the fluxes  $H^x$  and  $H^y$  at the boundary. As we set the slopes in all boundary cells to zero, the corresponding fluxes are given by

$$\begin{aligned} H_{\frac{1}{2}, k}^{n,x} &= -\alpha_{1,k}^n v_{1,k}^n - B_{1,k}^x, & H_{M+\frac{1}{2}, k}^{n,x} &= -\alpha_{M,k}^n v_{M,k}^n - B_{M,k}^x \\ H_{i, \frac{1}{2}}^{n,y} &= -\beta_{i,1}^n v_{i,1}^n - B_{i,1}^y, & H_{i, M+\frac{1}{2}}^{n,y} &= -\beta_{i,M}^n v_{i,M}^n - B_{i,M}^y, \quad i, k \in \mathcal{M} \end{aligned}$$

**Case 2** (partially open table problem): we consider the partially open table problem in two-dimensions, where we choose the domain with wall boundaries as given in Fig.2 (b) (see [1]). In this scenario, the evolution of the solution  $u$  at the boundary vertices involves prescribing its values appropriately. For the solution  $v$ , we impose boundary conditions through numerical fluxes. The conditions for  $i, k \in \mathcal{M}$  are outlined in the following lines:

- Left vertical boundary

$$\begin{aligned} u_{\frac{1}{2}, k+\frac{1}{2}}^{n+1} &= u_{\frac{1}{2}, k+\frac{1}{2}}^n + h \max(\alpha_{\frac{1}{2}, k+\frac{1}{2}}^n, 0) \\ H_{\frac{1}{2}, j}^{n,x} &= \begin{cases} -\alpha_{1,k}^n v_{1,k}^n - B^x(x_1, y_k), & \text{if } \alpha_{1,k}^n \geq 0 \\ -B^x(x_0, y_k) & \text{otherwise} \end{cases} \end{aligned}$$

- Right vertical boundary

$$\begin{aligned} u_{M+\frac{1}{2}, k+\frac{1}{2}}^{n+1} &= u_{M-\frac{1}{2}, k+\frac{1}{2}}^n + h \max(\alpha_{M-1, k+\frac{1}{2}}^n, 0) \\ H_{M+\frac{1}{2}, k}^{n,x} &= \begin{cases} -\alpha_{M,k}^n v_{M,k}^n - B^x(x_M, y_k), & \text{if } \alpha_{M,k}^n \leq 0 \\ -B^x(x_{M+1}, y_k) & \text{otherwise} \end{cases} \end{aligned}$$

- Bottom horizontal boundary

$$\begin{aligned} u_{i+\frac{1}{2}, \frac{1}{2}}^{n+1} &= \begin{cases} 0 & \text{if } x_{i+\frac{1}{2}} \leq 0.5 \\ u_{i+\frac{1}{2}, \frac{3}{2}}^n + h \max(\beta_{i+\frac{1}{2}, 2}^n, 0) & \text{if } x_{i+\frac{1}{2}} > 0.5 \end{cases} \\ H_{i, \frac{1}{2}}^{n,y} &= \begin{cases} -\beta_{i,1}^n v_{i,1}^n - B^y(x_i, y_1), & \text{if } x_{i+\frac{1}{2}} \geq 0.5 \text{ and } \beta_{i,1} \geq 0 \\ -B^y(x_i, y_{-1}) & \text{if } x_{i+\frac{1}{2}} \geq 0.5 \text{ and } \beta_{i,1} < 0 \\ -\beta_{i,1}^n v_{i,1}^n - B^y(x_i, y_1), & \text{if } x_{i+\frac{1}{2}} > 0.5 \end{cases} \end{aligned}$$

- Top horizontal boundary

$$\begin{aligned} u_{i+\frac{1}{2}, M+\frac{1}{2}}^{n+1} &= u_{i+\frac{1}{2}, M-\frac{1}{2}}^n + h \max(\beta_{i+\frac{1}{2}, M-1}^n, 0) \\ H_{i, M+\frac{1}{2}}^{n,y} &= \begin{cases} -\beta_{i,M}^n v_{i,M}^n - B^y(x_i, y_M), & \text{if } \beta_{i,M}^n \leq 0 \\ -B^y(x_i, y_{M+1}) & \text{otherwise} \end{cases} \end{aligned}$$

Finally, at the corner vertices of the rectangular domain, solution  $u$  is computed by taking the average of solution computed through horizontal and vertical directions. Note that all the boundary conditions are imposed in each stage of the RK time stepping.

## 7 Numerical experiments

We denote by FO, SO and SO- $\Theta$  first-order, second-order and second-order adaptive schemes, respectively. Through out this section, we denote by  $\|\cdot\|_\infty$  and  $\|\cdot\|_1$ , the supremum norm and the  $L^1$  norm, respectively.

### 7.1 Examples in one-dimension (1D)

In this section, we study one-dimensional examples, specifically addressing the problem (6)-(7) with the source function given by

$$f(x) = 0.5, \text{ for all } x \in [0, 1] \quad (41)$$

in the computational domain  $[0, 1]$ . Further,  $u_s$  and  $v_s$  denote the exact steady state solutions and are given by

$$u_s(x) = \min(x, 1 - x), \quad x \in [0, 1]$$

$$v_s(x) = \begin{cases} \int_x^{\frac{1}{2}} f(\xi) d\xi & \text{if } x \in [0, \frac{1}{2}] \\ \int_{\frac{1}{2}}^x f(\xi) d\xi & \text{if } x \in (\frac{1}{2}, 1] \end{cases} \quad (42)$$

where  $f$  is the source function given by (41). We consider various test cases in 1D to understand the significance of the proposed SO- $\Theta$  scheme. The boundary conditions in each case are employed as detailed in Section 2.1 and 2.3. The initial conditions are set as  $u = 0$  and  $v = 0$  in  $[0, 1]$ .

**Example 1 (convergence test case-1D)** In this test case, we verify the experimental order of convergence (E.O.C.) of the proposed SO- $\Theta$  scheme away from the steady state and compare it with that of FO and SO schemes. The source function is given by (41). We compute the solution at time  $T = 1.3$  and numerical solutions are evolved with a time step  $\Delta t = 0.3h$  (i.e.,  $\lambda = 0.3$ ). Since the exact solution of the problem is not available away from the steady state, the E.O.C. is computed using a reference solution which is obtained by the SO scheme with a fine mesh of size  $\Delta x = 1/8000$ . We denote by  $u_r$  and  $v_r$  the reference solutions corresponding to  $u$  and  $v$ , respectively. The results are given in Table 1. From the definition of  $\Theta$  in (27), it becomes apparent that away from the steady state, both SO and SO- $\Theta$  schemes

$\Delta x$	$\ u_{\Delta x} - u_r\ _\infty$	E.O.C.	$\ v_{\Delta x} - v_r\ _1$	E.O.C.
FO scheme				
0.025	0.0122	-	0.0085	-
0.0125	0.0069	0.8122	0.0052	0.7100
0.00625	0.0040	0.7728	0.0032	0.7022
0.003125	0.0023	0.7941	0.0019	0.7899
0.0015625	0.0013	0.8098	0.0011	0.7655
SO scheme				
0.025	0.0058	-	0.0049	-
0.0125	0.0028	1.03110	0.0024	1.0023
0.00625	0.0014	1.0422	0.0012	1.0237
0.003125	0.0007	1.0483	0.0006	1.0473
0.0015625	0.0003	1.0656	0.0003	0.9933
SO- $\Theta$ scheme				
0.025	0.0062	-	0.0050	-
0.0125	0.0030	1.0674	0.0025	1.0395
0.00625	0.0014	1.0655	0.0012	1.0031
0.003125	0.0007	1.0633	0.0006	1.0423
0.0015625	0.0003	1.0749	0.0003	1.0053

Table 1: Example 1 (1D): errors of numerical solutions produced by FO, SO and SO- $\Theta$  schemes computed up to the final time  $t = 1.3$  with a time step of  $\Delta t = 0.3h$ .

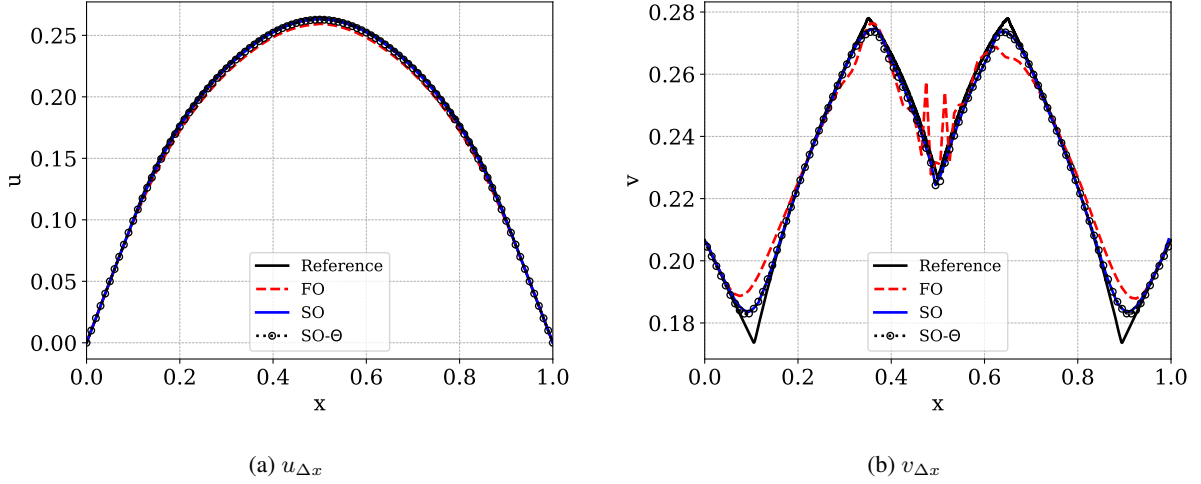


Figure 3: Example 1 (1D): numerical solutions computed at time  $t = 1.3$ , with  $\Delta x = 1/100$ ,  $\Delta t = 0.45\Delta x$ .

approach each other. This observation aligns with the findings from the numerical experiment, where both schemes exhibit nearly identical convergence rates.

Next, at the same time  $T = 1.3$ , we will compare the results for a larger CFL, say  $\lambda = 0.45$ , at a value within the permissible limit as in Theorem 1. The solutions corresponding to FO, SO and SO- $\Theta$  schemes with  $\Delta x = 1/100$  are compared against the same reference solution mentioned earlier. The results are given in Fig. 3. It is observed that, even though the FO scheme is stable with this  $\lambda = 0.45$ , it produces oscillations. This is in contrast to the SO and SO- $\Theta$  schemes. This indicates the robustness of the proposed SO- $\Theta$  schemes with larger values of  $\lambda$  away from the steady state.

**Example 2 (well balance test case-1D)** The purpose of this example is to illustrate the well-balance property of

$\Delta x$	$\ u_{\Delta x} - \bar{u}\ _{\infty}$	$\ v_{\Delta x} - \bar{v}\ _1$
FO scheme		
0.02	6.9388e-18	7.0546e-18
0.01	1.3878e-17	8.7499e-17
0.005	1.3878e-17	9.4632e-17
0.0025	6.9389e-18	1.2179e-15
SO scheme		
0.02	6.9389e-18	0.0001
0.01	6.9389e-18	3.4875e-05
0.005	1.3878e-17	8.7188e-06
0.0025	6.9389e-18	2.1797e-06
SO- $\Theta$ scheme		
0.02	6.9389e-18	5.3950e-17
0.01	6.9389e-18	6.7966e-17
0.005	1.3878e-17	7.2185e-17
0.0025	6.9389e-18	6.6996e-16

Table 2: Example 2 (1D): well-balance test for FO, SO and SO- $\Theta$  schemes. Numerical errors produced by FO, SO and SO- $\Theta$  schemes in a single time step, i.e., at the final time  $T = \Delta t$  with  $\Delta t = 0.45\Delta x$ .

the SO- $\Theta$  scheme for the problem (6)-(7). The simulations are carried out for a single time step, i.e.,  $T = \Delta t$ , with  $\lambda = 0.45$ , where the initial condition is set as the exact steady state solution (42).

We compute the errors  $\|u_{\Delta x} - u_s\|_{\infty}$  and  $\|v_{\Delta x} - v_s\|_1$  for various values of  $\Delta x$  and present the results in Table 2. It is observed that the SO- $\Theta$  scheme achieves the well-balance property, consistent with the FO scheme. In contrast, the SO scheme fails to capture this well-balance property. This observation agrees with the result in Lemma 2.

**Example 3 (steady state solution test case-1D)** In this example, we compute numerical solutions with the initial condition  $u_0 = 0$  and  $v_0 = 0$ , and evolve them up to the steady state level using the FO, SO and SO- $\Theta$  schemes. For all

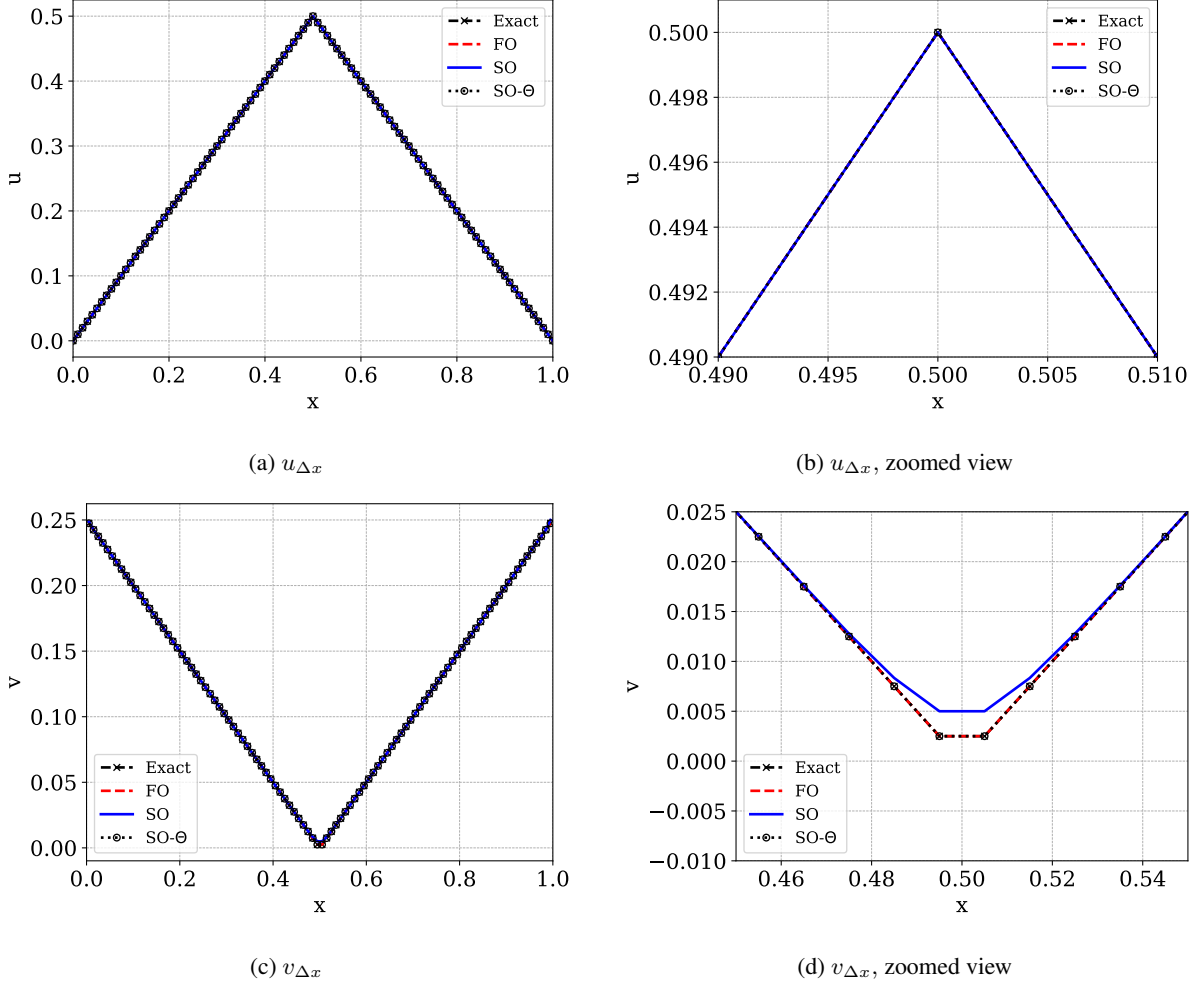


Figure 4: Example 3 (1D): numerical solutions near the steady state, computed at time  $T = 450$  with  $\Delta x = 1/100$ ,  $\Delta t = 0.45\Delta x$ . (b) and (d) are enlarged view of (a) and (c), respectively.

the three schemes, the numerical solutions are computed at  $T = 450$  with  $\lambda = 0.45$  and  $\Delta x = 1/100$ . The numerical results are then compared with the exact steady state solution (42), which are plotted through interpolation on the same mesh  $\Delta x = 1/100$  and are given in Fig. 4. The obtained results reveal that the FO and the adapted SO- $\Theta$  schemes align remarkably well with the steady state solution. On the other hand, the SO scheme, successfully reaches the steady state for  $u$  as shown in Fig. 4 (a) and (b), but it exhibits poor performance for  $v$ , as shown in Fig. 4 (c) and (d). This emphasizes the significance of the adaptation strategy when employing a second-order scheme to accurately capture the steady state solution.

**Example 4 (error versus number of iterations plots-1D)** In this example, we demonstrate the efficiency of the SO- $\Theta$  scheme in reaching the steady state solution by showing that it takes less number of iterations compared to the FO scheme. To assess this, we plot the errors  $\|u_{\Delta x} - u_s\|_{\infty}$  and  $\|v_{\Delta x} - v_s\|_1$  at each iteration against the number of iterations for solving the problem (6)-(7). Here also we keep the same  $\lambda = 0.45$  with a mesh size of  $\Delta x = 1/100$ . We compare the outcomes from the FO, SO and SO- $\Theta$  schemes. The results are depicted in Fig. 5. It is crucial to emphasize that the SO- $\Theta$  scheme reverts to first-order at the steady state. When comparing the solution  $u$ , the SO scheme shows better performance than both the FO and SO- $\Theta$  schemes, but not in  $v$ . The key challenge here is in achieving the steady state for  $v$ . In this context, the results reveal the efficiency of the SO- $\Theta$  scheme, which converges to the steady state with lesser iterations than the FO scheme, Fig. 5 (a) and (b). Significantly, the non-adaptive SO scheme encounters difficulties in reaching the steady state for  $v$ . In conclusion, the SO- $\Theta$  scheme performs better compared to the FO scheme.

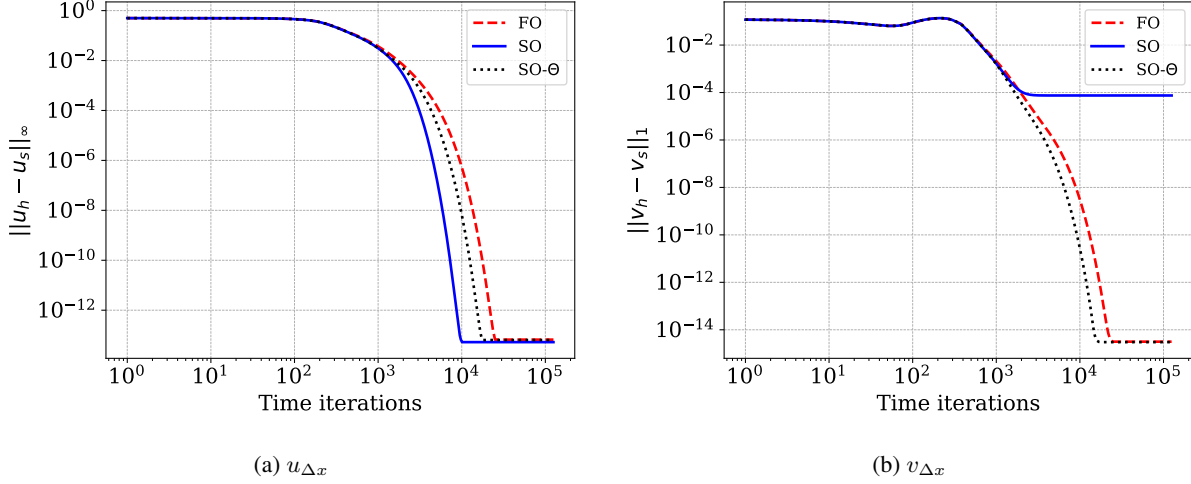


Figure 5: Example 4 (1D): numerical errors versus number of time iterations plots. Numerical solutions are computed till it reach near the state with  $\Delta x = 1/100$ ,  $\Delta t = 0.45h$ . In each iteration, the errors produced by FO, SO and SO- $\Theta$  schemes are compared.

## 7.2 Examples in two-dimensions (2D)

We perform numerous numerical experiments in a two-dimensional setting, employing a computational domain  $[0, 1] \times [0, 1]$ . As mentioned previously, we discretize this domain into uniform Cartesian grids, denoted as  $h = \Delta x = \Delta y$ . Our focus here centers on investigating SO- $\Theta$  scheme for three specific types of problems in the two-dimensional context: those involving a complete source, scenarios with a discontinuous source, and problems related to partially open boundaries, detailed in [1, 3]. The boundary conditions for each examples in this test cases are described in Section 6.4 and the initial conditions are set as  $u = 0$  and  $v = 0$  in  $(0, 1) \times (0, 1)$ . In all the examples below we take the source function as  $f = 0.5$  on  $[0, 1] \times [0, 1]$ .

**Example 5 (convergence test case-2D)** Here, for the open table problem, we analyze the E.O.C. of SO- $\Theta$  scheme with respect to the steady state solution and compare it with the FO and SO schemes. The numerical solutions are computed

h	$\ u_{\Delta x} - u_r\ _\infty$	E.O.C.	$\ v_{\Delta x} - v_r\ _1$	E.O.C.
FO scheme				
0.05	0.0662	-	0.0031	-
0.025	0.0334	0.9841	0.0009	1.7513
0.0125	0.0167	1.0037	0.0002	1.8799
0.00625	0.0084	0.9876	6.4819e-05	1.9368
SO scheme				
0.05	0.0599	-	0.0038	-
0.025	0.0299	0.9992	0.0017	1.1327
0.0125	0.0150	0.9994	0.0008	1.0709
0.00625	0.0075	0.9986	0.0004	1.0385
SO- $\Theta$ scheme				
0.05	0.0600	-	0.0018	-
0.025	0.0300	0.9995	0.0005	1.9026
0.0125	0.0150	0.9991	0.0001	1.9178
0.00625	0.0075	0.9984	3.3913e-05	1.9059

Table 3: Example 5 (2D): numerical errors produced by FO, SO and SO- $\Theta$  schemes, computed up to time  $T = 26$  with the time step  $\Delta t = 0.35h$ .

near the steady state, by running the simulation till the time  $T = 26$ , as studied in [3]. Considering the value  $\lambda = 0.7$  used in [3] for the FO scheme, we adopt a natural choice for the SO and SO- $\Theta$  schemes with  $\lambda = 0.35$ . Here, for a fair

comparison, we use the same  $\lambda = 0.35$  for all the three schemes FO, SO and SO- $\Theta$ . The E.O.C. is computed as:

$$\varphi(h) := \log\left(\frac{e(h)}{e(h/2)}\right) / \log 2,$$

where  $e(h)$  denotes  $\|u_{\Delta x} - u_s\|_\infty$  and  $\|v_{\Delta x} - v_s\|_1$  in respective cases. The outcomes presented in Table 3 reveal that the SO- $\Theta$  scheme exhibits marginally superior convergence when compared with the FO scheme despite the fact that the SO- $\Theta$  scheme reduces to the FO scheme in the vicinity of the steady state. On the other hand, it is evident that the SO scheme displays a diminished rate of convergence in comparison to both the FO and SO- $\Theta$  schemes for  $v$ . This emphasizes the robustness and significance of the proposed SO- $\Theta$  scheme.

Next, to visualize the solution near the steady state, we run the simulation till the time  $T = 196$ , with the same  $\lambda = 0.35$  and  $h = 1/50$ . We plot the approximate solutions obtained using the FO and SO- $\Theta$  schemes with the exact steady solutions in Fig. 6, where exact steady state solutions are plotted with linear interpolation on a finer mesh of size  $\Delta x = 0.5$ . Since the approximate solutions are very close to the steady state solutions, visual distinctions are difficult to discern from the given plots.

**Example 6 (error versus number of iterations-2D)** We examine the error versus number of iterations plot obtained using the FO, SO, and SO- $\Theta$  schemes for the open table problem. To conduct this comparison, as for Example 5, we take  $\lambda = 0.35$  with a mesh size of  $h = 1/50$ . Errors  $\|u_{\Delta x} - u_s\|_\infty$  and  $\|v_{\Delta x} - v_s\|_1$ , are computed at each iteration and plotted against the number of iterations. The results depicted in Fig. 7 clearly indicate that the SO- $\Theta$  scheme outperforms the FO and SO schemes. In other words, the SO- $\Theta$  scheme converges to the steady state more rapidly in comparison to the FO and SO schemes, demonstrating its superior efficiency.

**Example 7 (solutions at finite time-2D)** Here again we consider the open table problem and compare the solution profiles at a finite time, specifically at  $T = 3.0$ . The main aim here is to show that the SO- $\Theta$  scheme performs well even for the larger  $\lambda$ . We compute the approximate solution  $v_h$  using both the FO and SO- $\Theta$  schemes and plot with contour curves. The computations are performed for different values of  $\lambda$ : 0.35, 0.45, and 0.7, all with a mesh size of  $h = 1/50$  and the results are given in Fig. 9. For  $\lambda = 0.35$ , we see a clear distinction between the two schemes. In the case of  $v$ : the FO scheme exhibits oscillations, particularly noticeable when observing the contour plots along the lines  $\{(x, y) : x = 0.5, 0 \leq y \leq 1\}$  and  $\{(x, y) : y = 0.5, 0 \leq x \leq 1\}$  in Fig. 9 (a) and (b). In contrast, the SO- $\Theta$  scheme generates fewer oscillations, indicating its robustness. Furthermore, as the value of  $\lambda$  increase to 0.45 and 0.7, the oscillations intensify in the FO schemes. However, the SO- $\Theta$  scheme remains stable and less-oscillatory. This is evident in Fig. 9 (b), (d) and (f). In the case of  $u$ : we observe this same behaviour at time  $T = 1.2$ , which is given in Fig. 8. This comparison highlights the robustness of the SO- $\Theta$  scheme in producing accurate solutions at finite times, emphasizing its significance in numerical simulations.

**Example 8 (discontinuous source test case-2D)** In this example we consider the open table problem in the computational domain  $[0, 1] \times [0, 1]$  with a discontinuous source function given by (see Example 2 of [3], page no. 1110)

$$f(x, y) = \begin{cases} 0.5 & \text{if } (x, y) \in D_f, \\ 0 & \text{elsewhere,} \end{cases}$$

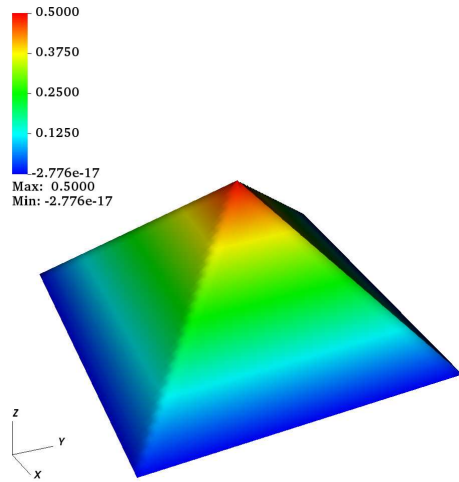
where  $D_f := [0.1, 0.3] \times [0.5, 0.7] \cup [0.5, 0.7] \times [0.7, 0.9]$ . The decomposition of source function  $f$  is as given in [3]. As explained in [3], the discretization of the domain  $[0, 1] \times [0, 1]$  is carefully done such that corners of the interior squares (see Fig. 21 in [3]) fall at the center of the computational cell. Due to this reason, in this test case we choose a mesh size of  $h = 1/55$ . For more details on this experiment we refer to [3]. We compute the solutions at large time  $T = 200$ , where it reaches the steady state with  $\lambda = 0.35$ . The results are printed in Fig. 10. It is evident that the SO- $\Theta$  scheme produces a better sharp resolution near the crest formation compared to the FO scheme.

**Example 9 (partially open table problem-2D)** We consider the domain  $(0, 1) \times (0, 1)$  with the boundary walls  $\Gamma_w$  and open boundary  $\Gamma_o$  as given in Fig. 2 (b). In this scenario, we aim to solve the problem defined by equations (1)-(4), with a given source function

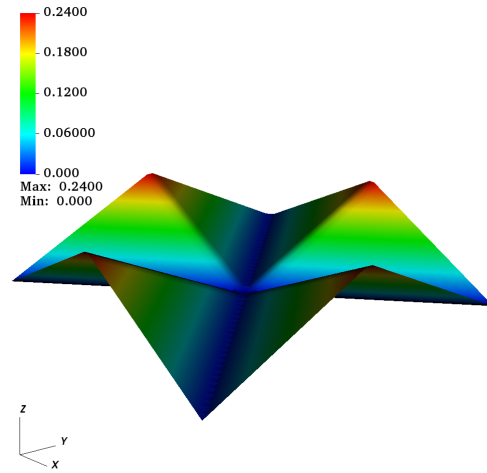
$$f(x, y) = 0.5 \text{ for all } (x, y) \in [0, 1] \times [0, 1].$$

Further details about the source decomposition and problem description can be found in [1]. The computations are performed with a mesh size  $h = 1/50$  and  $\lambda = 0.1$ . It is worth noting that we have opted here a relatively small value of  $\lambda$  in comparison to the previous examples. This is due to the fact that solution  $v$  takes larger values, and  $\lambda$  has to satisfy the condition:  $\lambda \max_i v_i^n \leq 1/2$  of Theorem 1. The simulations are done using both the FO and SO- $\Theta$  schemes until a large time  $T = 200$ , allowing the numerical solutions to approach the steady state. For this example, the exact steady state solutions are available and are given by

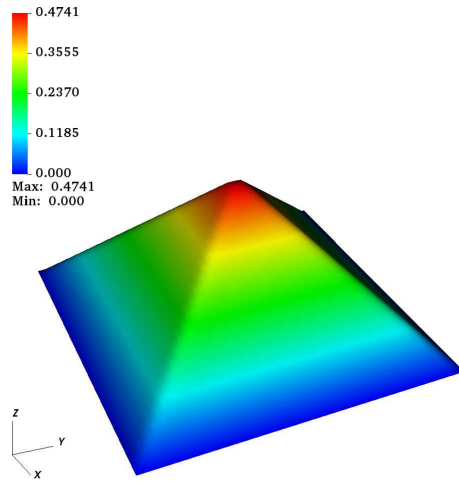
$$u_s(x, y) = \begin{cases} y & \text{if } x \leq 0.5, \\ \sqrt{(x - \frac{1}{2})^2 + y^2} & \text{if } x > 0.5, \end{cases}, \quad v_s(x, y) = \begin{cases} 1 - y & \text{if } x \leq 0.5, \\ \frac{1}{d_\Gamma(x, y)} \int_{d_\Gamma(x, y)}^{l(x, y)} \rho d\rho & \text{if } x > 0.5, \end{cases}$$



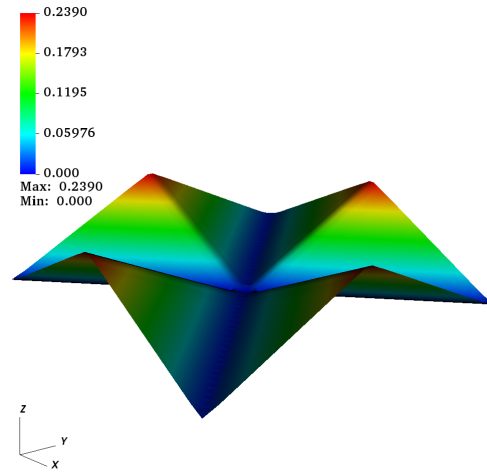
(a)  $u$  : exact steady state solution



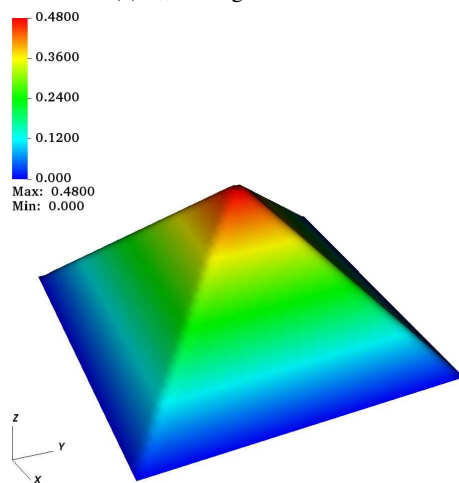
(b)  $v$  : exact steady state solution



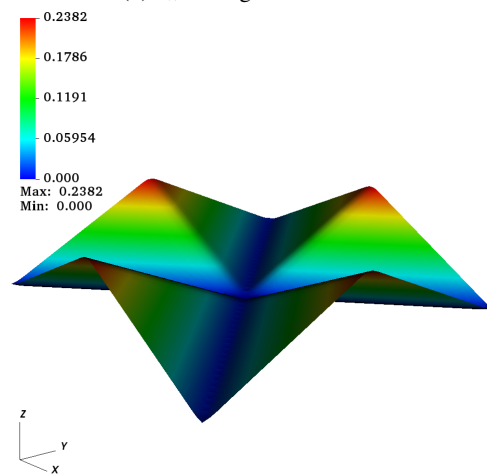
(c)  $u_h$  : using FO scheme



(d)  $v_h$  : using FO scheme



(e)  $u_h$  : using SO- $\Theta$  scheme



(f)  $v_h$  : using SO- $\Theta$  scheme

Figure 6: Example 5 (2D): numerical solutions near the steady state computed with  $h = 1/50$  and  $\Delta t = 0.35h$  at final time  $T = 196$ .

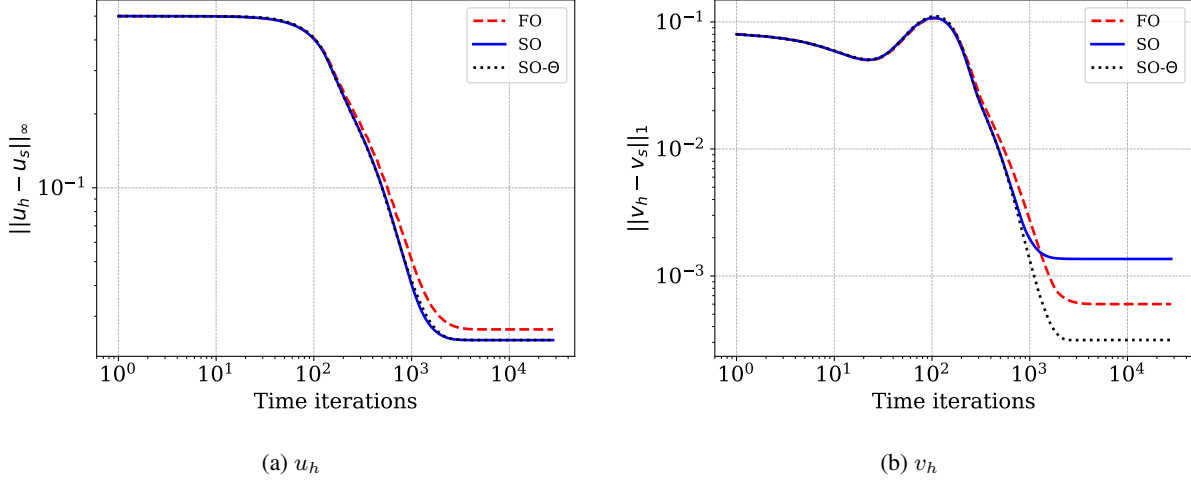


Figure 7: Example 6 (2D): numerical errors versus number of time iterations plots for the open table problem with  $h = 1/50$  and  $\Delta t = 0.35h$ . Numerical solutions are evolved till they reach near the steady state.

where

$$l(x, y) = \begin{cases} \sqrt{(1 - \frac{1}{2})^2 + (\frac{0.5y}{x - \frac{1}{2}})^2} & \text{if } \frac{y}{x - \frac{1}{2}} \leq \frac{1}{0.5}, \\ \sqrt{1 + (\frac{x - \frac{1}{2}}{y})^2} & \text{if } \frac{y}{x - \frac{1}{2}} > \frac{1}{0.5}, \end{cases}, \quad d_{\Gamma}(x, y) = \sqrt{(x - \frac{1}{2})^2 + y^2}$$

These solutions are plotted using the linear interpolation on a mesh of size  $h = 1/200$ . The comparison of numerical solutions obtained from the FO and SO- $\Theta$  schemes with the exact steady state solutions is presented in Fig. 11 and 12. The results are visualized using 40 contour curves in Fig. 12. Notably, in the vicinity of the point  $(0.5, 0)$  where the solution  $v_h$  exhibits a singularity, the SO- $\Theta$  scheme provides significantly better resolutions compared to the FO scheme. This enhancement is particularly evident when comparing the numerical solutions with the exact steady state solution. These results clearly demonstrate the advantage of the SO- $\Theta$  scheme over the FO scheme in the partially open table test case.

## 8 Conclusion

In this study, we address the challenges associated with numerically approximating the Hadler and Kuttler (**HK**) model, a complex system of non-linear partial differential equations describing granular matter dynamics. Focusing on second-order schemes, we study the issues such as initial oscillations and delays in reaching steady states. We present a second-order scheme that incorporates a MUSCL-type spatial reconstruction and a strong stability preserving Runge-Kutta time-stepping method, building upon the first-order scheme. Through an adaptation procedure that employs a modified limiting strategy in the linear reconstruction, our scheme achieves the well-balance property. We extend our analysis to two dimensions and demonstrate the effectiveness of our adaptive scheme through numerical examples. Notably, our resulting scheme significantly reduces initial oscillations, reaches the steady state solution faster than the first-order scheme, and provides a sharper resolution of the discrete steady state solution.

## Acknowledgement

This work was done while one of the authors, G. D. Veerappa Gowda, was a Raja Ramanna Fellow at TIFR-Centre for Applicable Mathematics, Bangalore. The work of Sudarshan Kumar K. is supported by the Science and Engineering Research Board, Government of India, under MATRICS project no. MTR/2017/000649.

## References

- [1] ADIMURTHI, A. AGGARWAL, AND G. D. V. GOWDA, *Godunov-type numerical methods for a model of granular flow on open tables with walls*, Commun. Comput. Phys., 20 (2016), pp. 1071–1105.



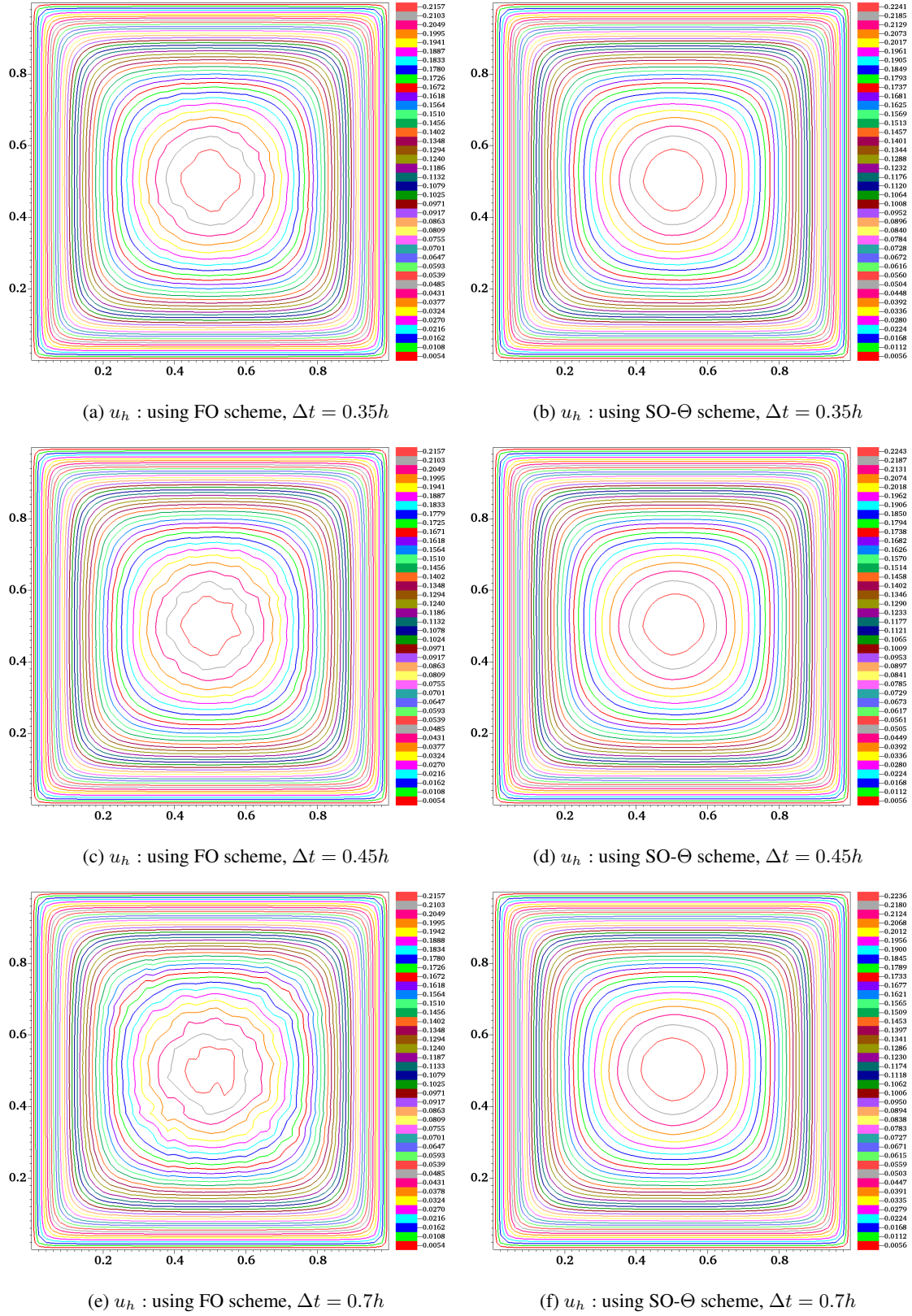


Figure 8: Example 7 (2D): numerical solutions computed at time  $T = 1.2$  with a mesh size  $h = 1/50$  and using values of  $\lambda : 0.35, 0.45$  and  $0.7$ . The contour plots use 40 contour curves.

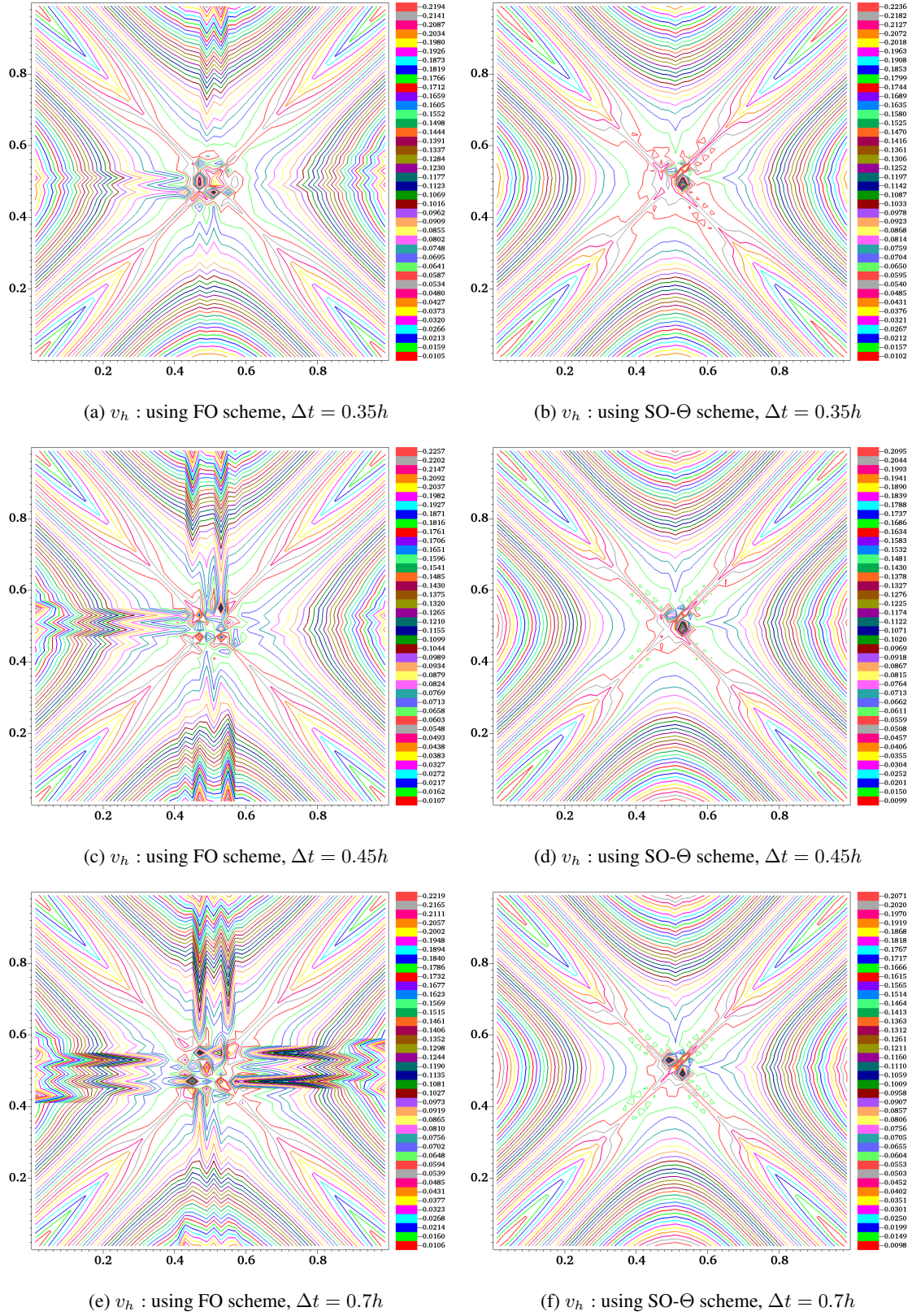


Figure 9: Example 7 (2D): numerical solutions computed at time  $T = 3.0$  with a mesh size  $h = 1/50$  and using values of  $\lambda$ : 0.35, 0.45 and 0.7. The contour plots use 40 contour curves.

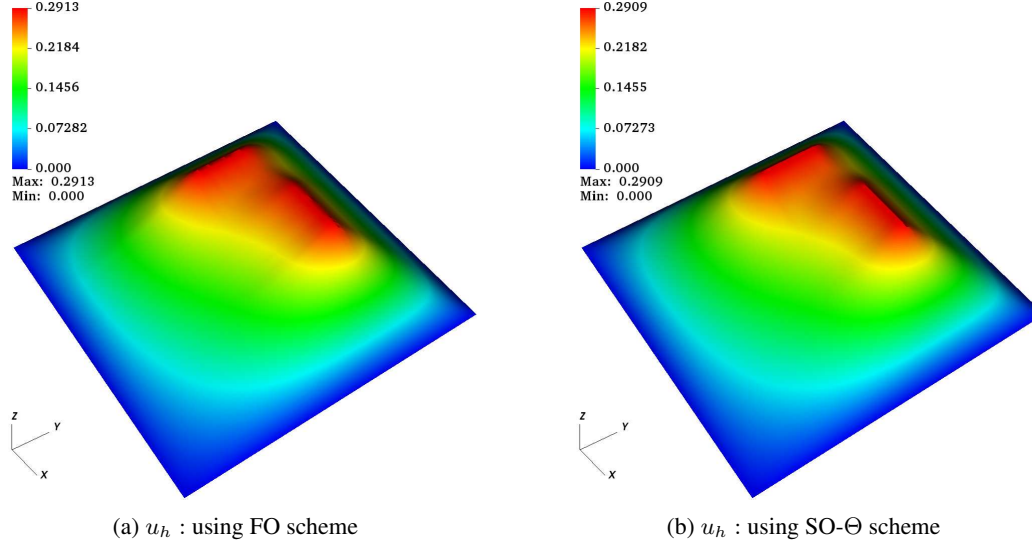
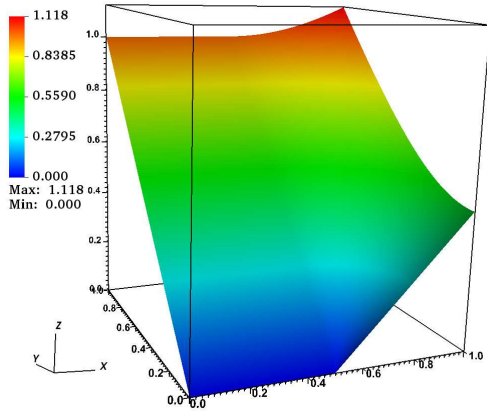
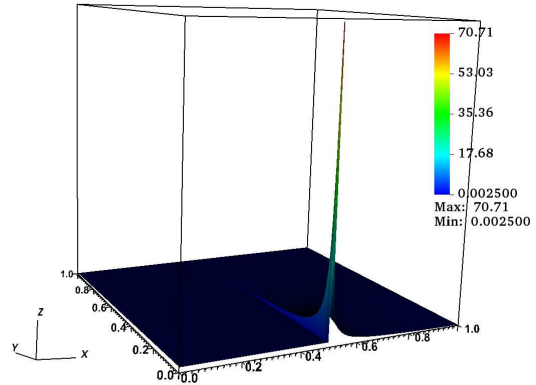


Figure 10: Example 8 (2D): numerical solutions corresponding to a discontinuous source, computed at time  $T = 200$  with  $h = 1/55$  and  $\Delta T = 0.35h$ .

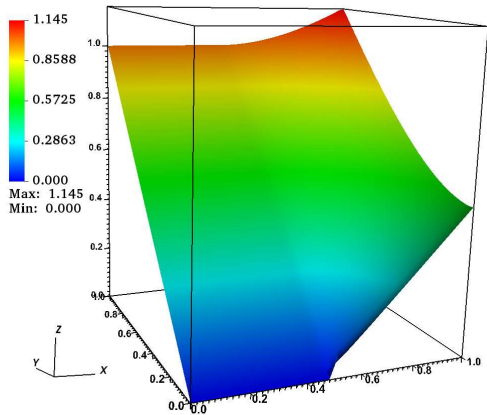
- [2] ADIMURTHI, S. KUMAR K., AND G. D. VEERAPPA GOWDA, *On the convergence of a second order approximation of conservation laws with discontinuous flux*, Bull. Braz. Math. Soc. (N.S.), 47 (2016), pp. 21–35.
- [3] A. ADIMURTHI, A. AGGARWAL, AND G. D. VEERAPPA GOWDA, *Godunov-type numerical methods for a model of granular flow*, J. Comput. Phys., 305 (2016), pp. 1083–1118.
- [4] D. AMADORI AND W. SHEN, *Global existence of large BV solutions in a model of granular flow*, Comm. Partial Differential Equations, 34 (2009), pp. 1003–1040.
- [5] D. AMADORI AND W. SHEN, *Mathematical Aspects of A Model for Granular Flow*, in Nonlinear Conservation Laws and Applications, Springer, 2011, pp. 169–179.
- [6] D. AMADORI AND W. SHEN, *Front tracking approximations for slow erosion*, Discrete Contin. Dyn. Syst., 32 (2012), pp. 1481–1502.
- [7] A. BERMUDEZ AND M. E. VAZQUEZ, *Upwind methods for hyperbolic conservation laws with source terms*, Comput. & Fluids, 23 (1994), pp. 1049–1071.
- [8] C. BERTHON AND C. CHALONS, *A fully well-balanced, positive and entropy-satisfying Godunov-type method for the shallow-water equations*, Math. Comp., 85 (2016), pp. 1281–1307.
- [9] A. BRESSAN AND W. SHEN, *A semigroup approach to an integro-differential equation modeling slow erosion*, J. Differential Equations, 257 (2014), pp. 2360–2403.
- [10] R. BÜRGER, S. K. KENETTINKARA, R. RUIZ BAIER, AND H. TORRES, *Coupling of discontinuous Galerkin schemes for viscous flow in porous media with adsorption*, SIAM J. Sci. Comput., 40 (2018), pp. B637–B662.
- [11] R. BÜRGER, S. KUMAR, K. SUDARSHAN KUMAR, AND R. RUIZ-BAIER, *Discontinuous approximation of viscous two-phase flow in heterogeneous porous media*, J. Comput. Phys., 321 (2016), pp. 126–150.
- [12] P. CANNARSA AND P. CARDALIAGUET, *Representation of equilibrium solutions to the table problem for growing sandpiles*, J. Eur. Math. Soc. (JEMS), 6 (2004), pp. 435–464.
- [13] P. CANNARSA, P. CARDALIAGUET, G. CRASTA, AND E. GIORGIERI, *A boundary value problem for a PDE model in mass transfer theory: representation of solutions and applications*, Calc. Var. Partial Differential Equations, 24 (2005), pp. 431–457.
- [14] P. CANNARSA, P. CARDALIAGUET, AND C. SINISTRARI, *On a differential model for growing sandpiles with non-regular sources*, Comm. Partial Differential Equations, 34 (2009), pp. 656–675.
- [15] G. M. COCLITE AND E. JANNELLI, *Well-posedness for a slow erosion model*, J. Math. Anal. Appl., 456 (2017), pp. 337–355.
- [16] R. COLOMBO, G. GUERRA, AND F. MONTI, *Modelling the dynamics of granular matter*, IMA Journal of Applied Mathematics, 77 (2012), pp. 140–156.



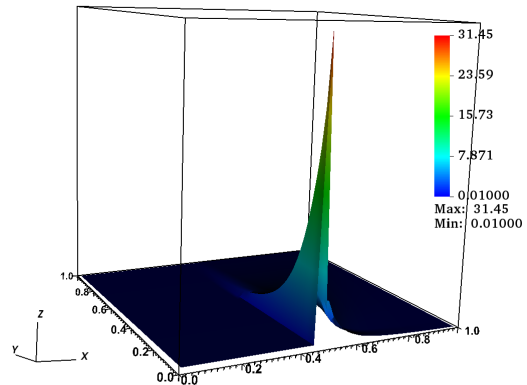
(a)  $\bar{u}$  : exact steady state solution



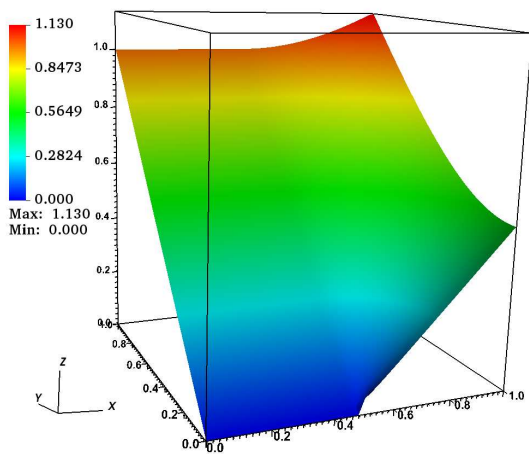
(b)  $\bar{v}$  : exact steady state solution



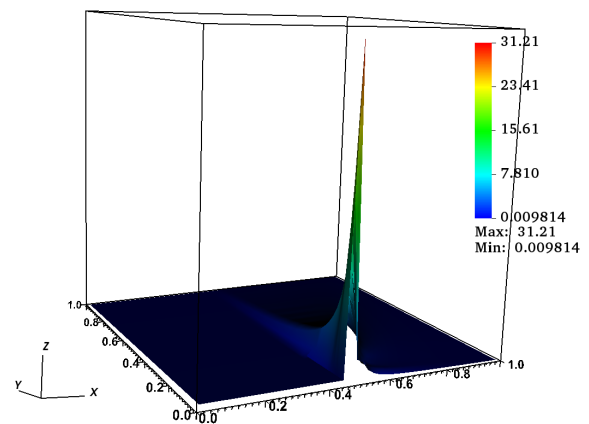
(c)  $u_h$  : using FO scheme



(d)  $v_h$  : using FO scheme



(e)  $u_h$  : using SO- $\Theta$  scheme



(f)  $v_h$  : using SO- $\Theta$  scheme

Figure 11: Example 9 (2D): numerical solutions of partially open table problem with  $h = 1/50$  and  $\Delta t = 0.1h$  computed at the final time  $T = 200$ .

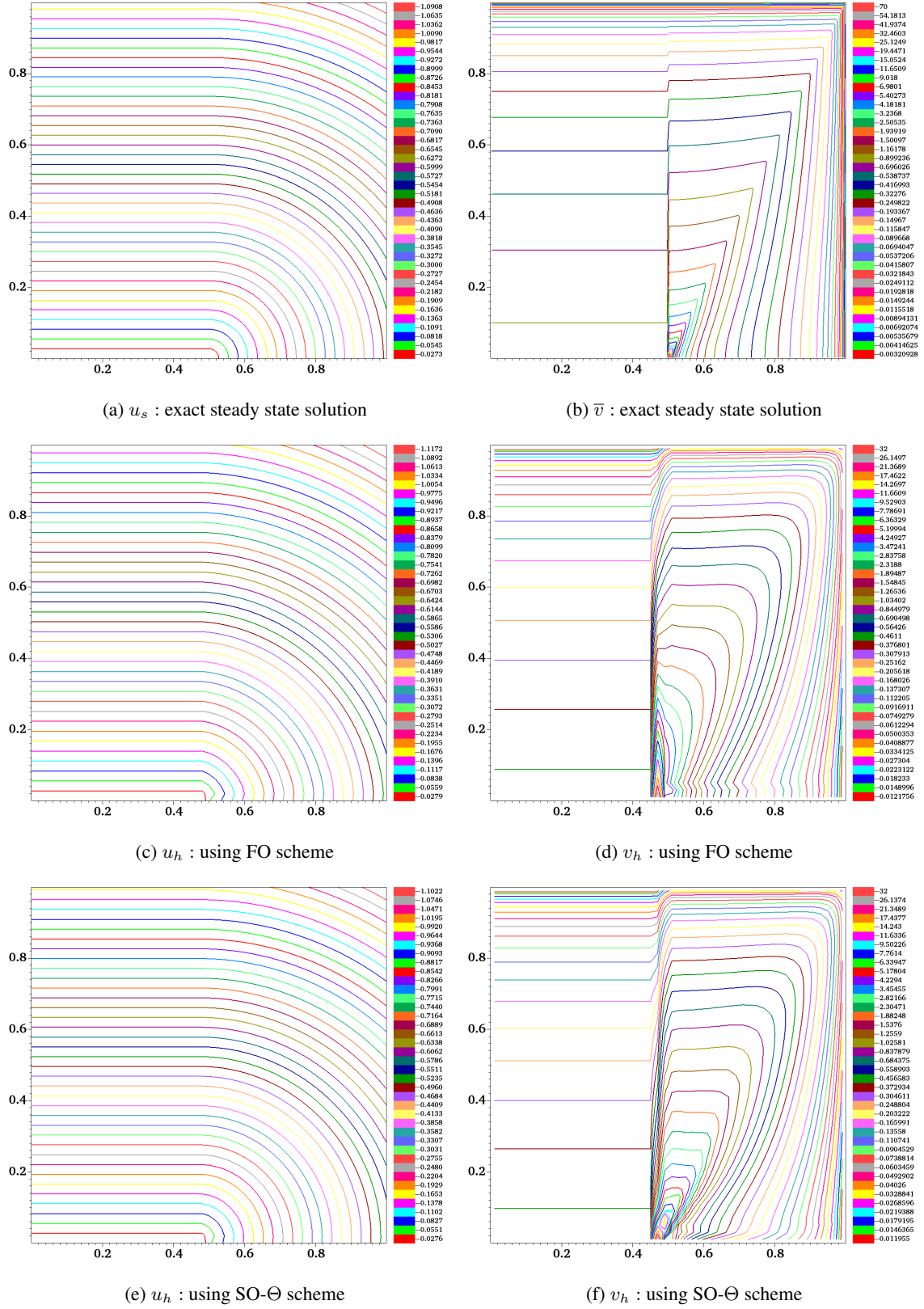


Figure 12: Example 9 (2D): numerical solutions of partially open table problem computed at the final time  $T = 200$  with  $h = 1/50$ ,  $\Delta t = 0.1h$ . The contour plots use 40 contour curves.

- [17] R. M. COLOMBO, G. GUERRA, AND W. SHEN, *Lipschitz semigroup for an integro-differential equation for slow erosion*, *Quart. Appl. Math.*, 70 (2012), pp. 539–578.
- [18] G. CRASTA AND S. FINZI VITA, *An existence result for the sandpile problem on flat tables with walls*, *Netw. Heterog. Media*, 3 (2008), pp. 815–830.
- [19] V. DESVEAUX AND A. MASSET, *A fully well-balanced scheme for shallow water equations with Coriolis force*, *Commun. Math. Sci.*, 20 (2022), pp. 1875–1900.
- [20] M. FALCONE AND S. FINZI VITA, *A finite-difference approximation of a two-layer system for growing sandpiles*, *SIAM J. Sci. Comput.*, 28 (2006), pp. 1120–1132.
- [21] M. FALCONE AND S. FINZI VITA, *A semi-Lagrangian scheme for the open table problem in granular matter theory*, in *Numerical mathematics and advanced applications*, Springer, Berlin, 2008, pp. 711–718.
- [22] S. FINZI VITA, *Numerical simulation of growing sandpiles*, *Control Systems: Theory, Numerics and Applications*, CSTNA2005, (2005).
- [23] B. GHITTI, C. BERTHON, M. H. LE, AND E. F. TORO, *A fully well-balanced scheme for the 1D blood flow equations with friction source term*, *J. Comput. Phys.*, 421 (2020), pp. 109750, 33.
- [24] L. GOSSE, *A well-balanced flux-vector splitting scheme designed for hyperbolic systems of conservation laws with source terms*, *Comput. Math. Appl.*, 39 (2000), pp. 135–159.
- [25] S. GOTTLIEB AND C.-W. SHU, *Total variation diminishing runge-kutta schemes*, *Math. Comput.*, 67 (1998), pp. 73–85.
- [26] S. GOTTLIEB, C.-W. SHU, AND E. TADMOR, *Strong stability-preserving high-order time discretization methods*, *SIAM Review*, 43 (2001), pp. 89–112.
- [27] J. GREENBERG AND A.-Y. LEROUX, *A well-balanced scheme for the numerical processing of source terms in hyperbolic equations*, *SIAM Journal on Numerical Analysis*, 33 (1996), pp. 1–16.
- [28] G. GUERRA AND W. SHEN, *Existence and stability of traveling waves for an integro-differential equation for slow erosion*, *J. Differential Equations*, 256 (2014), pp. 253–282.
- [29] K. HADELER AND C. KUTTLER, *Dynamical models for granular matter*, *Granular matter*, 2 (1999), pp. 9–18.
- [30] A. HARTEN, P. D. LAX, AND B. VAN LEER, *On upstream differencing and Godunov-type schemes for hyperbolic conservation laws*, *SIAM Rev.*, 25 (1983), pp. 35–61.
- [31] V. MICHEL-DANSAC, C. BERTHON, S. CLAIN, AND F. FOUCHER, *A well-balanced scheme for the shallow-water equations with topography*, *Comput. Math. Appl.*, 72 (2016), pp. 568–593.
- [32] L. PRIGOZHIN, *Variational model of sandpile growth*, *European Journal of Applied Mathematics*, 7 (1996), pp. 225–235.
- [33] W. SHEN, *On the shape of avalanches*, *Journal of Mathematical Analysis and Applications*, 339 (2008), pp. 828–838.
- [34] K. SUDARSHAN KUMAR, C. PRAVEEN, AND G. D. VEERAPPA GOWDA, *A finite volume method for a two-phase multicomponent polymer flooding*, *J. Comput. Phys.*, 275 (2014), pp. 667–695.
- [35] B. VAN LEER, *Towards the ultimate conservative difference scheme. v. a second-order sequel to godunov's method*, *J. Comput. Phys.*, 32 (1979), pp. 101–136.